Supporting Information for

Low Melting Non-corrosive Asymmetric Thioether-TFSI Li Salts for Solid Polymer Electrolytes

Vladislav Y. Shevtsov[a,b], Francesco Gambino[c,d], Daniil R. Nosov[a], Jérôme Guillot[e], Silvia Porporato[c,d], Giuseppe A. Elia[c,d], Claudio Gerbaldi[c,d]*, Alexander S. Shaplov[a]*

[a] *Functional Polymeric and Particulate Materials Unit, Luxembourg Institute of Science and Technology (LIST), 28 avenue des Hauts-Fourneaux, L-4362 Esch-sur-Alzette, Luxembourg*

[b] *Department of Physics and Materials Science, University of Luxembourg, L-4365 Esch-sur-Alzette, Luxembourg*

[c] *GAME Lab, Department of Applied Science and Technology (DISAT), Politecnico di Torino, 24 Corso Duca degli Abruzzi, 10129 Torino, Italy*

[d] *National Reference Center for Electrochemical Energy Storage (GISEL), 9 Via G. Giusti, 50121 Firenze, Italy*

[e] *Advanced Analyses and Support Unit, Luxembourg Institute of Science and Technology (LIST), 28 avenue des Hauts-Fourneaux, L-4362 Esch-sur-Alzette, Luxembourg*

Correspondence:
Email: claudio.gerbaldi@polito.it
Email: alexander.shaplov@list.lu,

Experimental

Materials

2-Chloroethanesulfonyl chloride (98%, Acros Organics), trifluoromethanesulfonylamide ($CF_3SO_2NH_2$, 97%, ABCR), triethylamine (TEA, for synthesis, Merck), diisopropylamine (DIPA, ≥99.5%, Sigma-Aldrich), 2,2,2-trifluoroethanethiol (95%, Sigma-Aldrich), 2-(2-methoxyethoxy)ethane-1-thiol (97%, Sigma-Aldrich), lithium tetrafluoroborate ($LiBF_4$, 99%, Acros Organics), phosphorus pentoxide (P_2O_5, Sicapent®, Merck), and activated charcoal (Acros Organics) were used as received. Acetonitrile (AcN, anhydrous, 99.5%, Acros Organics), methanol (MeOH, anhydrous, 99.5%, Acros Organics), ethyl acetate (EtAc, 99%, Fisher), diethylether (Et_2O, 99%, Fisher), dichloromethane (DCM, 99.5%), hexafluorobenzene

(C_6F_6, 99%, Acros Organics) and acetone (99%, Fisher) were utilized without additional purification.

Potassium carbonate (K_2CO_3, 99.2%, BLDpharm) was dried at 140 °C for 6 h before use. Dimethyl sulfoxide-d_6 (DMSO-d_6, 99.9 atom%D, Sigma-Aldrich) was dried over 4Å molecular sieves. Poly(ethylene oxide) - PEO (average molecular weight = $4 \cdot 10^5$ g mol^{-1}) and conductive carbon (Super C65) were sourced from Merck. Lithium iron phosphate ($LiFePO_4$) was obtained from BASF. Lithium bis(trifluoromethanesulfonyl)imide (LiTFSI), ethylene carbonate (EC) and dimethylene carbonate (DMC) battery grade were obtained from Solvionic.

Methods

Prior to all measurements, the salts were thoroughly dried at 50 °C/0.15 mbar for 12 h in a Büchi glass drying oven equipped with a P_2O_5 moisture trap. The dried samples were then transferred under vacuum into an argon-filled MBRAUN MB-Labstar glovebox (H_2O and O_2 content <0.5 ppm) and stored there for at least 5 days before further investigation.

Nuclear Magnetic Resonance (NMR)

NMR spectra were recorded on AMX-600 (Bruker) spectrometer at 25°C in the indicated deuterated solvent and are listed in ppm. The signals corresponding to the residual protons and carbons of the deuterated solvent were used as an internal standard for ^1H and ^{13}C NMR, respectively. The C_6F_6 (−164.9 ppm) was utilized as an external standard for ^{19}F NMR. Two-Dimensional NMR (2D NMR) analyses were additionally performed to confirm the molecular structure of more complex salts. Heteronuclear Single Quantum Coherence (HSQC), and Heteronuclear Multiple-bond Correlation (HMBC) 2D spectra are given with preference of proton traces being reported as X-axis and carbon traces as Y-axis.

Thermogravimetric analysis (TGA)

TGA of ILs was carried out in air on a TGA2 STARe System (Mettler Toledo) applying a heating rate of 5 °C min^{-1}. The onset weight loss temperature (T_{onset}) was determined as the point in the TGA curve at which a significant deviation from the horizontal was observed and then rounded to the nearest 5°C.

Differential Scanning Calorimetry (DSC)

DSC analysis was performed on a DSC 300 Caliris Select differential calorimeter (NETZSCH) in the range of −70 to 250°C for Li salts and between -90 and 180°C for Li salt/PEO SPEs. Samples were hermetically sealed in Al pans inside the argon-filled glove-box (MBRAUN MB-Labstar, H_2O and O_2 content < 0.5 ppm). Three heating-cooling cycles with a heating rate of

5, 5 and 10 °C min^{-1} were carried out for each sample under N_2 atmosphere. For the **Li salts** melting points (T_m) were determined from the first heating cycle at 5°C min^{-1} rate, while glass transition temperatures (T_g) were obtained from the heating curve of the second heating/cooling cycle at the same rate. For the **Li salt/PEO** solid polymer electrolytes, both the T_g and T_m were determined from the heating curve of the second heating/cooling cycle conducted at 5°C min^{-1} rate.

Electrochemical characterization

Total ionic conductivity (σ_{total}) of Li salt/PEO solid polymer electrolytes was determined by electrochemical impedance spectroscopy (EIS), using a VMP3 potentiostat/galvanostat (Bio-Logic Science Instruments). To avoid any influence of moisture/ humidity on the conductivity of polymer electrolytes, the latter were preliminary dried at 80 °C/0.1 mbar for 12 h in the B-585 oven (Buchi Glass Drying Oven) filled with P_2O_5 and were transferred under vacuum inside an argon-filled glovebox (MBRAUN MB-Labstar, H2O and O2 content<0.5 ppm). A polymer disk of 16 mm in diameter, with a thickness of about 120 µm, was sandwiched between two stainless-steel (SS) blocking electrodes in an SS||**Li salt/PEO**||SS configuration using EL-Cell model electrochemical test cells (EL-Cell Std). For each SPE, the thickness was accurately measured before and after tests using a micrometer (Mitutoyo). The closed cell was taken out of the glovebox and EIS experiments were carried by applying a sinusoidal voltage of 20 mV in the frequency range from 0.1 to 1×10^6 Hz and in a temperature range from 20 to 80 °C. Temperature was controlled using MK 53 E2 climatic chamber (Binder), where cells were allowed to reach thermal equilibrium for at least 45 min before each test.

The anodic electrochemical stability (oxidative stability) was evaluated at 70 °C by linear sweep voltammetry (LSV) using a VMP3 potentiostat/galvanostat (Bio-Logic Science Instruments). Test cells were assembled inside an argon-filled glovebox in a Li||**Li salt/PEO** ||carbon-coated Al (CC-Al) configuration. LSV measurements were conducted by scanning from the open-circuit voltage ((E_{ocv}) to 6.0 V at a scan rate of 0.1 mV s^{-1}.

The lithium-ion transference number (t_{Li^+}) was determined at 70 °C using a symmetric Li||**Li salt/PEO**||Li cell subjected to a 100 mV polarization bias (ΔV) with the aim to measure the initial (I_o) and steady-state (I_s) currents. EIS was carried out on a VMP3 potentiostat/galvanostat (Bio-Logic Science Instruments) by applying a 20 mV AC perturbation over the frequency range of 300 kHz to 0.01 Hz under open-circuit voltage (OCV) conditions. Impedance spectra were recorded both before and after polarization, and the lithium-ion transference number was calculated using the standard Bruce-Vincent-Evans method[1]:

$$t_{Li^+} = \frac{I_s(\Delta V - I_0 R_0)}{I_0(\Delta V - I_s R_s)}$$

where R_0 is the impedance resistance before polarization; R_s is the impedance after DC polarization; I_0 is the initial current; I_s is the final current after polarization, and ΔV represents the applied polarization voltage (20 mV).

Lithium plating/stripping tests were conducted at 70 °C using a symmetric Li‖**Li salt/PEO**‖Li cell configuration. The delivered capacity was fixed at 0.20 mAh, corresponding to a constant current density of 0.025 mA cm^{-2} applied for 8 h during plating and 8 h during stripping. Rate-dependent measurements were performed by varying the current density between 0.025, 0.050, 0.100, and 0.200 mA cm^{-2} while maintaining the same areal capacity (0.20 mAh). This testing protocol was also employed for long-term lithium plating/stripping cycling experiments at 70 °C.

Anodic dissolution tests were carried out using a two-electrode configuration (EL-Cell Std), with a pristine aluminum disc as working electrode and an oversized AC disc as counter electrode. A Whatman GF/A glass wool disk soaked with 150 µL of electrolyte was used for each test. During the measurement, the potential of the aluminum discs was increased 1.3 V over the open circuit potential and subsequently reverted at a scan rate of 5 mV s^{-1}. The potential was held for 3 h at the upper potential limit of each cycle.

X-Ray Photoelectron Spectroscopy (XPS) was performed on aluminum disks after the anodic dissolution tests using a Thermofisher Nexsa G2 instrument equipped with a monochromatic X-ray beam (Al K_α, E = 1486.6 eV), and working with 60 W (30 W respectively) power for an X-ray spot size of 200 µm (100 µm respectively). Survey scans were acquired using pass energy = 200 eV, step size = 1 eV; Narrow scans: using pass energy = 50 eV, step size = 0.1 eV. Photoelectron emission take-off angle was set to 0° with respect to the surface angle. Normal Binding Energy was referenced on the C-(C,H) component @ 285.0 eV. The samples were transferred into the analysis chamber from argon-filled glovebox using a special, hermetically sealed shuttle under inert atmosphere.

Batteries assembly and testing

SPE preparation

SPEs were prepared using a solvent-free method. PEO was manually blended mixed with the corresponding lithium salt in a mortar at a molar ratio of 20:1. After obtaining a homogeneous powder, the mixture was hot-pressed between two polypropylene sheets at 70 °C under 10 bar of pressure, yielding uniform, homogeneous and self-standing films. These films were cut into 16 mm disks and dried overnight at 50 °C under dynamic vacuum in a Buchi oven, then

transferred to an argon-filled glove box (Jacomex GP Campus with O_2 and H_2O levels < 0.8 ppm).

Composite cathode (catholyte) preparation

To prepare a cathode material the following composition was used: 60 wt.% of carbon coated $LiFePO_4$, 10 wt.% of C_{65} carbon black and 30 wt.% of binder material consisting of PEO and **Li salt** so that the ratio of EO units to Li is maintained at 20 : 1 by mol, respectively. Firstly, LFP active material powder and C_{65} carbon black were gently mixed in a hand mortar and, successively added to the ca. 5 wt.% solution of PEO and **Li salt** in acetonitrile upon stirring. The magnetic stirring continued at ambient temperature for 1 h, whereupon the resultant suspension was additionally homogenized using an Ultra-Turrax mixer (IKA-Werke GmbH & Co. KG) for 10 min. The obtained dense slurry was casted onto an aluminum current collector foil using a doctor-blade with a blade height of 300 μm. Acetonitrile solvent was removed by evaporation at ambient temperature for 12 h and further drying at 60 °C/1 mm Hg for 24 h in the B-585 oven (Buchi Glass Drying Oven) filled with P_2O_5. To avoid contamination with atmospheric moisture, the cathode tape was further transferred under vacuum inside the argon-filled glovebox. After drying, the obtained composite cathode films had a thickness of 100±2 μm and active mass loading of 2.8 ÷ 3 mg cm^{-2}.

In concrete examples, the compositions were 21.3 wt.% PEO and 8.7 wt.% Li TFT-TFSI for the **Li TFT-TFSI** salt, and 20.9 wt.% PEO and 9.1 wt.% Li MET-TFSI for the **Li MET-TFSI** salt.

Li cells assembly

Lab-scale Li°‖**Li salt/PEO**‖$LiFePO_4$ battery prototypes were assembled inside an Ar-filled glovebox using ECC-Std test cells (EL-Cell GmbH). A round Teflon spacer (100 μm thick, 12 mm inner diameter) was placed on top of the composite cathode tape, whereupon a layer of **Li salt/PEO** electrolyte was applied manually directly on the composite cathode surface within the internal diameter of the spacer. The assembly was completed by placing a lithium metal disk anode (14 mm diameter) on top of the Li salt/PEO electrolyte. As a result, the **Li salt/PEO** electrolyte layer thickness was defined by the Teflon spacer and measured 100 ± 5 μm.

Li cells testing

Lab-scale Li°‖**Li salt/PEO**‖$LiFePO_4$ half cells were galvanostatically cycled on a Arbin BT2000 battery tester at 70 °C. The cells were cycled between 2.5 and 3.8 V vs. Li^+/Li at different charge/discharge current regimes up to C/5, where the rate is denoted as C/n, corresponding to a full discharge or full charge of the theoretical cathode capacity (C = 170 mAh g^{-1}) in n hours.

Synthesis overview:

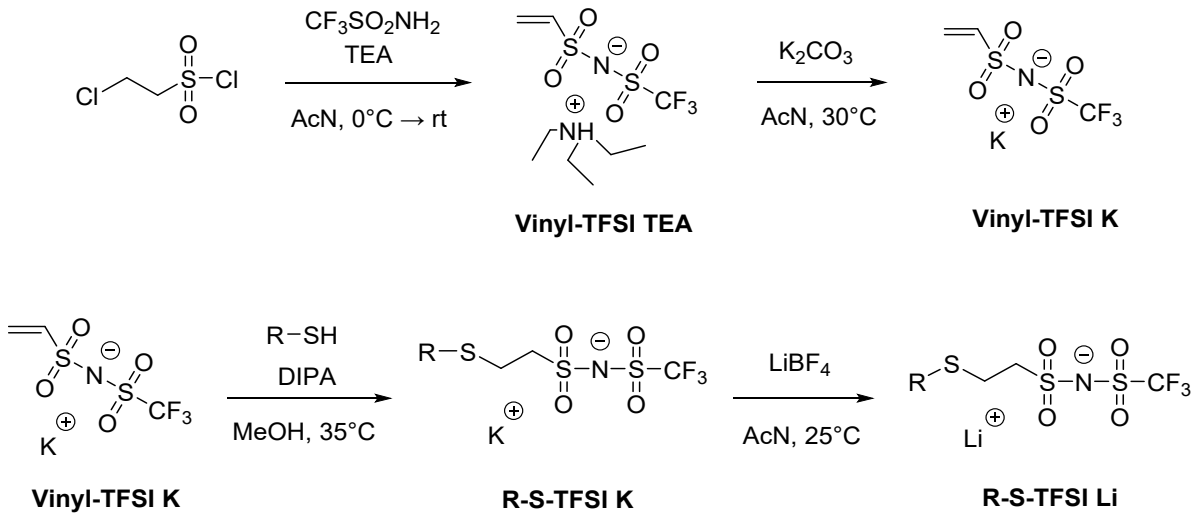

Scheme S1. General synthetic route for the preparation of **Li MET-TFSI** and **Li TFT-TFSI** salts.

Synthesis of **Vinyl-TFSI TEA**

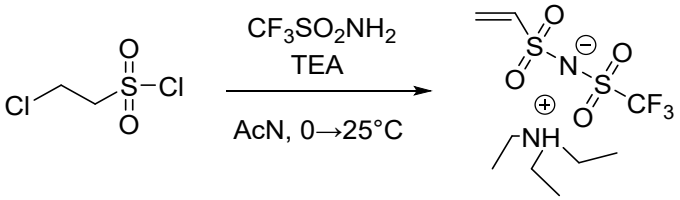

$CF_3SO_2NH_2$ (27.4 g, 0.184 mol) and triethylamine (TEA, 59.6 g, 0.589 mol) were dissolved in 60 mL of anhydrous acetonitrile (AcN) at room temperature (RT) under an inert atmosphere. The resulting solution was then precooled to 0 °C using an ice bath. A separate solution of 2-chloroethanesulfonyl chloride (30.0 g, 0.184 mol) in 200 mL of anhydrous AcN was prepared and added dropwise to the amine solution while maintaining the temperature at 0 °C. After the addition was complete, the ice bath was removed, and the reaction mixture was allowed to warm gradually to RT. Stirring was continued at 25 °C for 12 hours and the formation of a white precipitate of triethylammonium chloride ($(CH_3CH_2)_3NH^+Cl^-$) was observed. The precipitate was filtered off and the solvent was then evaporated. The resulting oil was dissolved in 50 mL of anhydrous ethyl acetate (EtAc) and the additional precipitation of $(CH_3CH_2)_3NH^+Cl^-$ was observed. The solid was filtered off, the solvent was subsequently removed under reduced pressure, yielding the brown oily product. It was finally dried at 40 °C/0.2 mbar for 12 h. Yield: 57.5 g (92 %); ^{1}H NMR (600 MHz, DMSO-d_6) δ 9.06 (s, 1H),

6.72 (dd, *J* = 16.6, 9.9 Hz, 1H), 5.89 (d, *J* = 16.6 Hz, 1H), 5.72 (d, *J* = 9.9 Hz, 1H), 3.09 (q, *J* = 7.4 Hz, 6H), 1.18 (t, *J* = 7.3 Hz, 9H).

Synthesis of **Vinyl-TFSI K**

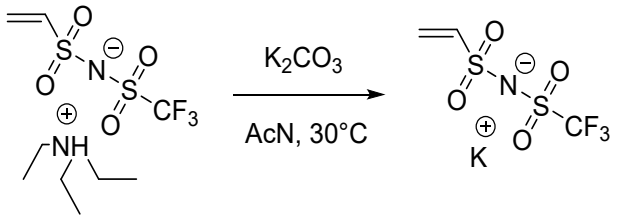

The freshly dried K_2CO_3 powder (58.3 g, 0.422 mol) was added in one portion to a solution of vinyl-TFSI TEA (57.5 g, 0.169 mol) in anhydrous AcN (200 mL). The suspension was then stirred for 12 h at 30°C under an inert atmosphere. The residual powder was filtered off and the solvent evaporated. The obtained beige powder was washed with anhydrous diethyl ether (3 × 35 mL) and further dried at 40°C/0.2 mbar for 15 h. Yield: 40.5 g (86 %); ^{1}H NMR (600 MHz, DMSO-d_6) δ 6.72 (dd, *J* = 16.6, 9.9 Hz, 1H), 5.89 (d, *J* = 16.6 Hz, 1H), 5.72 (d, *J* = 10.0 Hz, 1H).

Synthesis of **CF_3-CH_2-S-TFSI K**

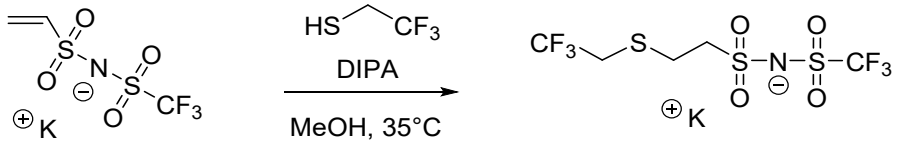

Vinyl-TFSI K (4.93 g, 17.8 mmol), 2,2,2-trifluoroethanethiol (2.68 g, 23.0 mmol), DIPA (0.36 g, 3.9 mmol), and anhydrous MeOH (20 mL) were charged into a high-pressure glass reactor, which was subsequently flushed with Ar and sealed. After complete dissolution at room temperature, the reaction mixture was stirred for 5 h at room temperature and then for an additional 15 h at 35 °C. Upon completion, the solution was concentrated to approximately half of its initial volume by evaporating 6 mL of methanol under reduced pressure (40 °C/100 mbar). The concentrated solution was then precipitated into an excess of anhydrous diethyl ether (60 mL) under vigorous stirring, affording beige powder. The solid was isolated by decantation, washed with anhydrous diethyl ether (3 × 25 mL), and dried at 30 °C/0.15 mbar for 12 h in a Büchi B-585 glass drying oven equipped with a P_2O_5 moisture trap. Yield: 4.80 g (68%); ^{1}H NMR (600 MHz, DMSO-d_6): δ = 3.55 (q, *J* = 10.7 Hz, 2H), 3.25 (p, 2H), 2.94 (p, 2H).

Synthesis of CF_3-CH_2-S-TFSI Li (**Li TFT-TFSI**)

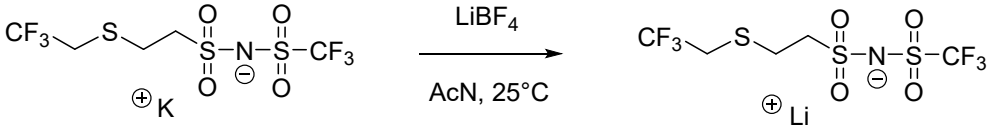

CF_3-CH_2-S-TFSI K (2.50 g, 6.3 mmol) and anhydrous $LiBF_4$ (0.60 g, 6.3 mmol) were dissolved in anhydrous acetonitrile (20 mL) under an argon atmosphere. The resulting solution was stirred at 25 °C for 24 h, during which the formation of a KBF_4 precipitate was observed. The suspension was subsequently filtered to afford a clear solution. The solvent was removed under reduced pressure to obtain white powder. The product was dried at 50 °C/0.1 mbar for 12 h in a Büchi B-585 glass drying oven equipped with a P_2O_5 moisture trap. Yield: 1.82 g (91 %); ^{1}H NMR (600 MHz, DMSO-d_6): δ = 3.55 (q, *J* = 10.7 Hz, 2H), 3.25 (p, 2H), 2.94 (p, 2H); ^{7}Li NMR (233 MHz, DMSO-d_6): δ = -1.05. ^{19}F NMR (565 MHz, DMSO-d_6): δ = -67.32 (t, *J* = 10.8 Hz), -79.80; Anal. calcd. for $C_5H_6F_6LiNO_4S_3$ (361.22): C, 16.63 %; H, 1.67 %; N, 3.88 %. Found: C, 16.69 %; H, 1.84 %; N, 3.98 % ; T_g = -2.9 °C (DSC, 5 °C min^{-1}); T_m = 135.9 °C (DSC, 5 °C min^{-1}).

Synthesis of **CH_3-(O-CH_2-CH_2)$_2$-S-TFSI K**

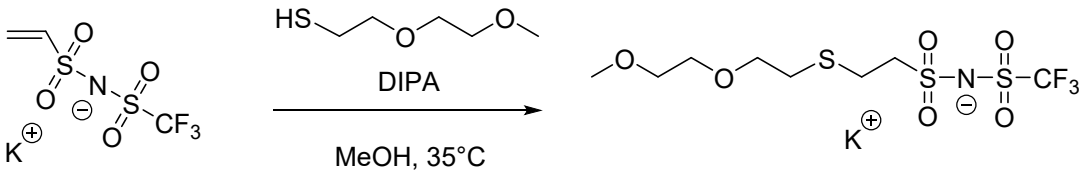

Vinyl-TFSI K (4.0 g, 14.4 mmol), 2-(2-methoxyethoxy)ethane-1-thiol (2.56 g, 18.7 mmol), DIPA (0.44 g, 4.3 mmol), and anhydrous MeOH (20 mL) were charged into a high-pressure glass reactor, which was subsequently flushed with Ar and sealed. After complete dissolution at room temperature, the reaction mixture was stirred for 5 h at room temperature and then for an additional 15 h at 35 °C. Upon completion, the solution was concentrated to approximately half of its initial volume by evaporating 7 mL of methanol under reduced pressure (40 °C/100 mbar). The concentrated solution was then precipitated into an excess of anhydrous diethyl ether (60 mL) under vigorous stirring, affording beige powder. The solid was isolated by decantation, washed with anhydrous diethyl ether (3 × 25 mL), and dried at 30 °C/0.15 mbar for 12 h in a Büchi B-585 glass drying oven equipped with a P_2O_5 moisture trap. Yield: 4.70 g (78%); ^{1}H NMR (600 MHz, DMSO-d_6): δ = 3.55 (t, *J* = 6.6 Hz, 2H), 3.53 - 3.50 (m, 2H), 3.45 - 3.42 (m, 2H), 3.24 (s, 3H), 3.20 (p, 2H), 2.80 (p, 2H), 2.69 (t, *J* = 6.6 Hz, 2H).

Synthesis of CH_3-(O-CH_2-CH_2)$_2$-S-TFSI Li (**Li MET-TFSI**)

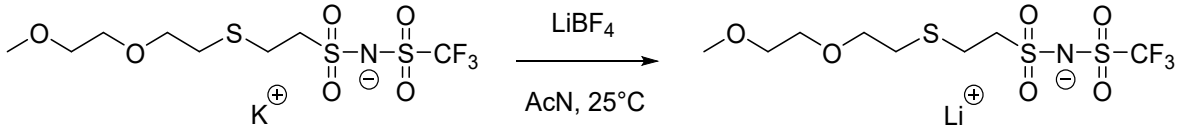

CH_3-(O-CH_2-CH_2)$_2$-S-TFSI K (4.70 g, 11.4 mmol) and anhydrous $LiBF_4$ (1.06 g, 11.4 mmol) were dissolved in anhydrous acetonitrile (40 mL) under an argon atmosphere. The resulting solution was stirred at 25 °C for 24 h, during which the formation of a KBF_4 precipitate was observed. The suspension was subsequently filtered to afford a clear solution. The solvent was removed under reduced pressure to obtain white powder. The product was dried at 50 °C/0.1 mbar for 12 h in a Büchi B-585 glass drying oven equipped with a P_2O_5 moisture trap. Yield: 3.7 g (89 %); ^{1}H NMR (600 MHz, DMSO-d_6): δ = 3.55 (t, *J* = 6.6 Hz, 2H), 3.53 - 3.50 (m, 2H), 3.45 - 3.42 (m, 2H), 3.24 (s, 3H), 3.20 (p, 2H), 2.80 (p, 2H), 2.69 (t, *J* = 6.6 Hz, 2H); ^{7}Li NMR (233 MHz, DMSO-d_6): δ = -1.04; ^{13}C NMR (151 MHz, DMSO-d_6): δ = 71.21, 69.96, 69.34, 57.83, 54.68, 30.50, 25.26; ^{19}F NMR (565 MHz, DMSO-d_6): δ = -79.80; Anal. calcd. for $C_8H_{15}F_3LiNO_6S_3$ (381.32): C, 25.20 %; H, 3.97 %; N, 3.67 %. Found: C, 24.57 %; H, 4.00 %; N, 3.68 % ; T_g = -3.9 °C (DSC, 5 °C min^{-1}); T_m = 71.4 °C (DSC, 5 °C min^{-1}).

Additional insights in the design of novel Li salts

Among the two proposed lithium salts, **Li TFT-TFSI** retains a CF_3 group content comparable to that of LiTFSI, whereas in **Li MET-TFSI** the fluorine content is reduced by approximately half.

Within the same chemical framework, the synthesis of asymmetric, fluorine-free lithium salts would be of considerable interest. Indeed, reducing fluorine content in lithium battery systems represents a clear and growing trend in electrochemical energy storage research. Several groups have already reported the development of fluorine-free lithium salts[2–5]. However, to the best of our knowledge, achieving stable, long-term cycling performance with fully fluorine-free electrolytes remains highly challenging. This is largely attributed to the exceptional thermal, chemical, and electrochemical stability, as well as the hydrophobic character, imparted by CF_3 groups.

In the present work, vinyl-TFSI K was reacted with two thiols via a thiol-ene Michael addition. The high efficiency of this click reaction (i.e., high yields and product purity) is partly due to the enhanced reactivity of the vinyl group induced by the strong electron-withdrawing -SO_2-CF_3 moiety. Removing this activating group would likely reduce the reactivity and complicate the synthetic pathway.

Finally, the motivation to synthesize thioether-containing compounds arises not only from the practicality of the synthetic route, namely, the simplicity of thiol-ene addition and the availability of vinyl-TFSI K, but also from a growing number of literature reports demonstrating that C–S–C linkages can impart advantageous properties to electrolytes for Li metal batteries[6–8]. These include a wider electrochemical stability window (vs Li/Li^+), higher Li^+ transference numbers, and, in some cases, enhanced ionic conductivity. Such improvements are often attributed to the intrinsic characteristics of the C–S bond, which is relatively long (~1.81 Å) compared to the C–O bond (~1.41–1.43 Å) and involves a less electronegative atom, thereby influencing chain flexibility and ion coordination behavior.

NMR Spectra

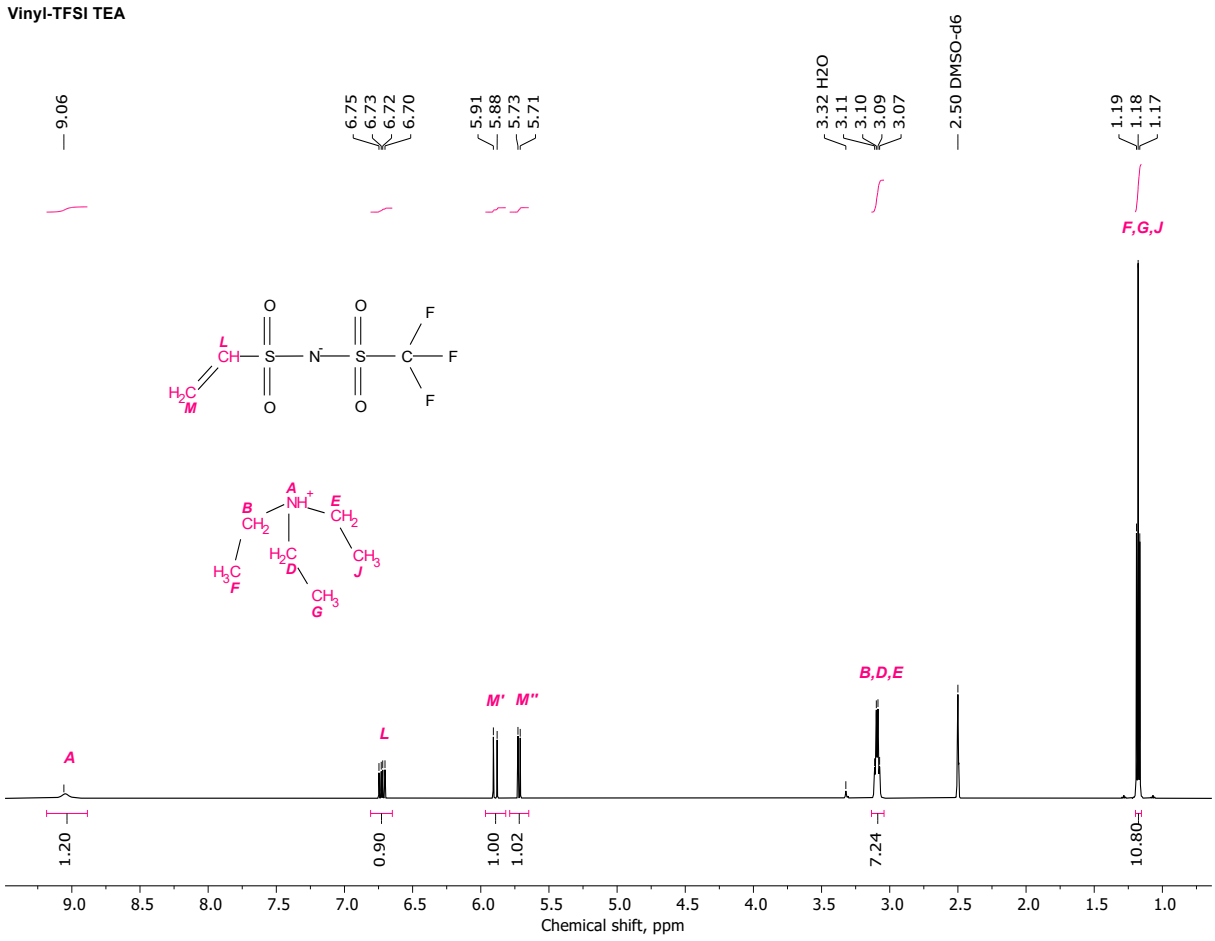

Figure S1. ^{1}H NMR spectrum of **Vinyl-TFSI TEA** (DMSO-d_6, 25.0 °C).

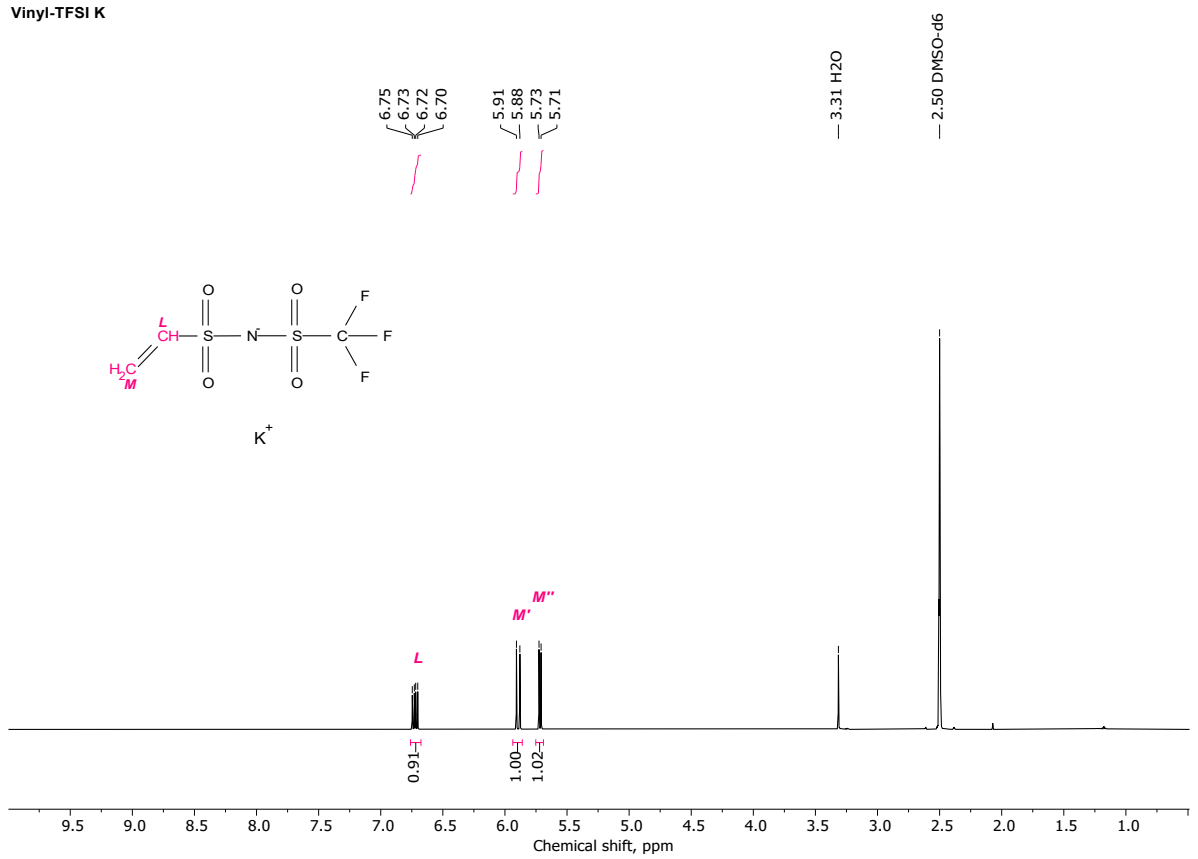

Figure S2. ^{1}H NMR spectrum of **Vinyl-TFSI K** (DMSO-d_6, 25.0 °C).

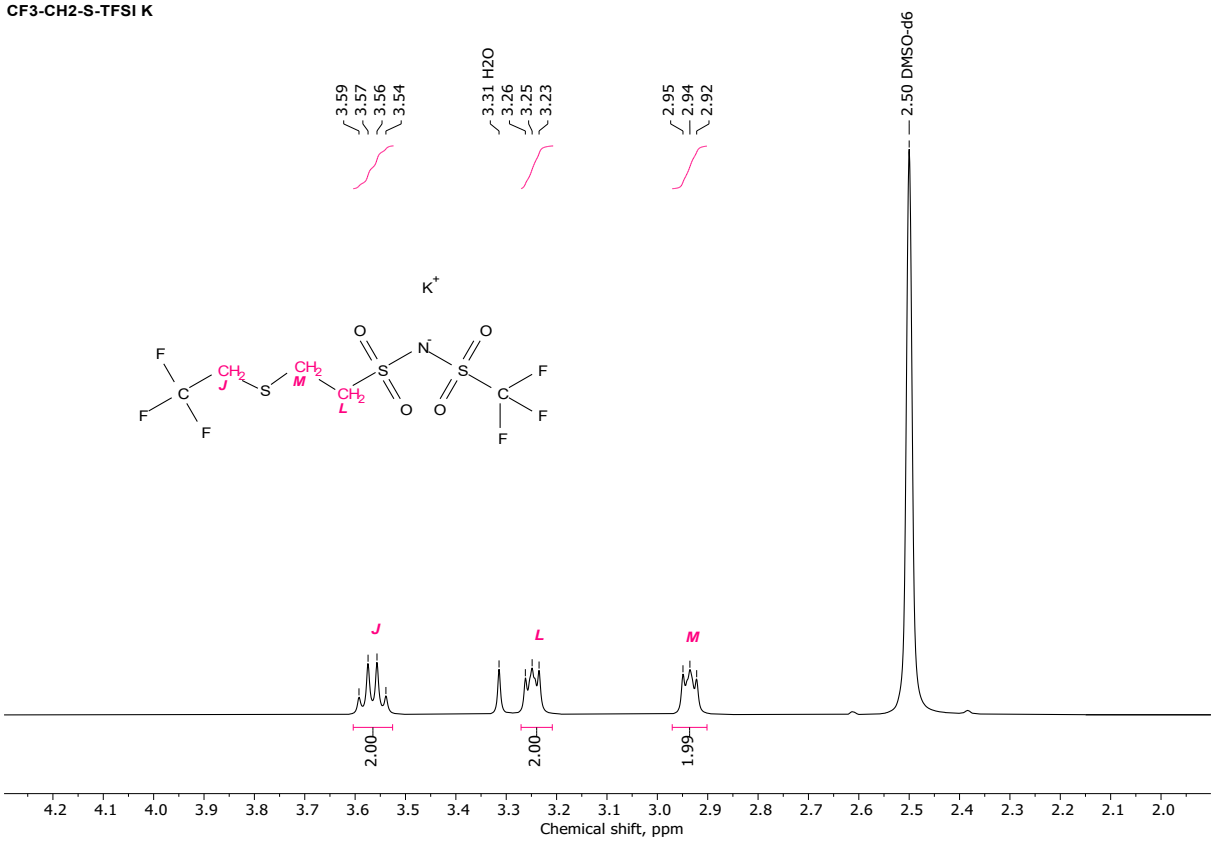

Figure S3. ^{1}H NMR spectrum of **CF_3-CH_2-S-TFSI K** (DMSO-d_6, 25.0 °C).

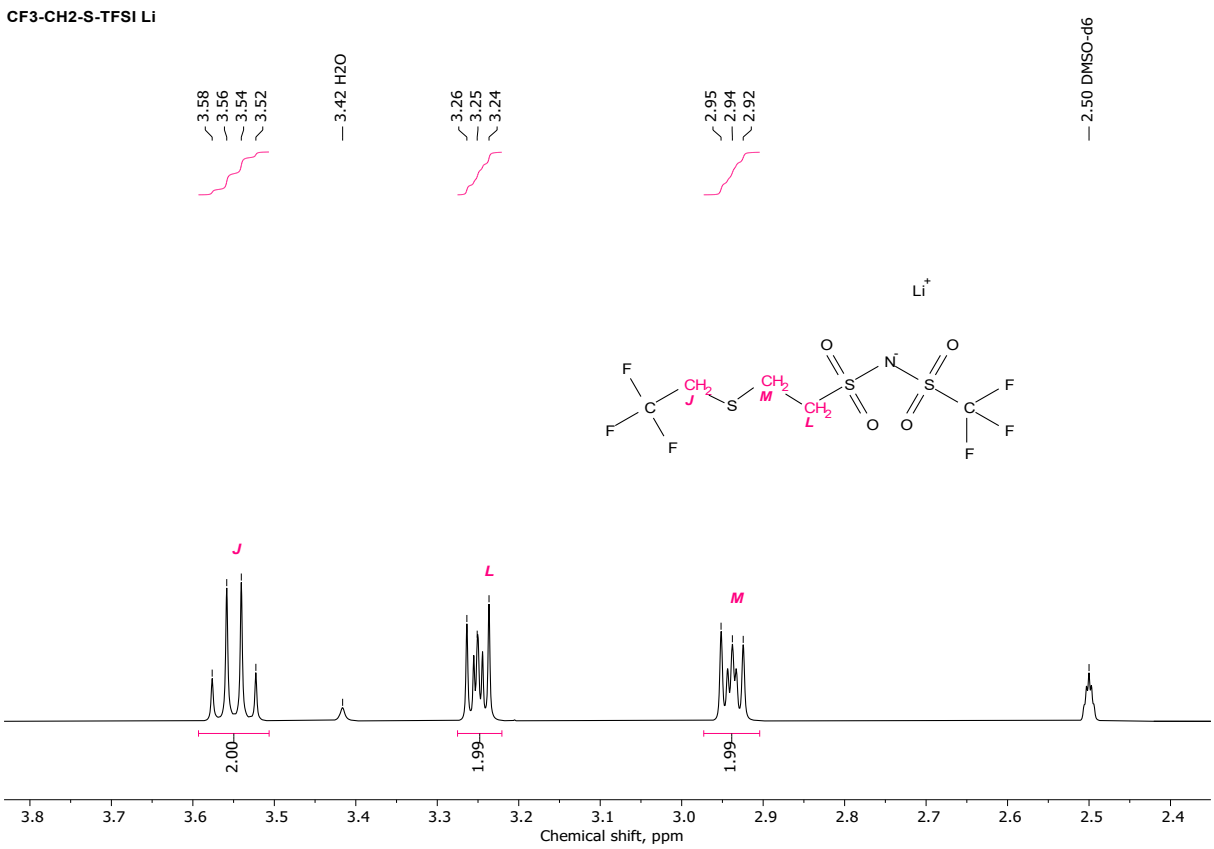

Figure S4. ^{1}H NMR spectrum of **Li TFT-TFSI** (DMSO-d_6, 25.0 °C).

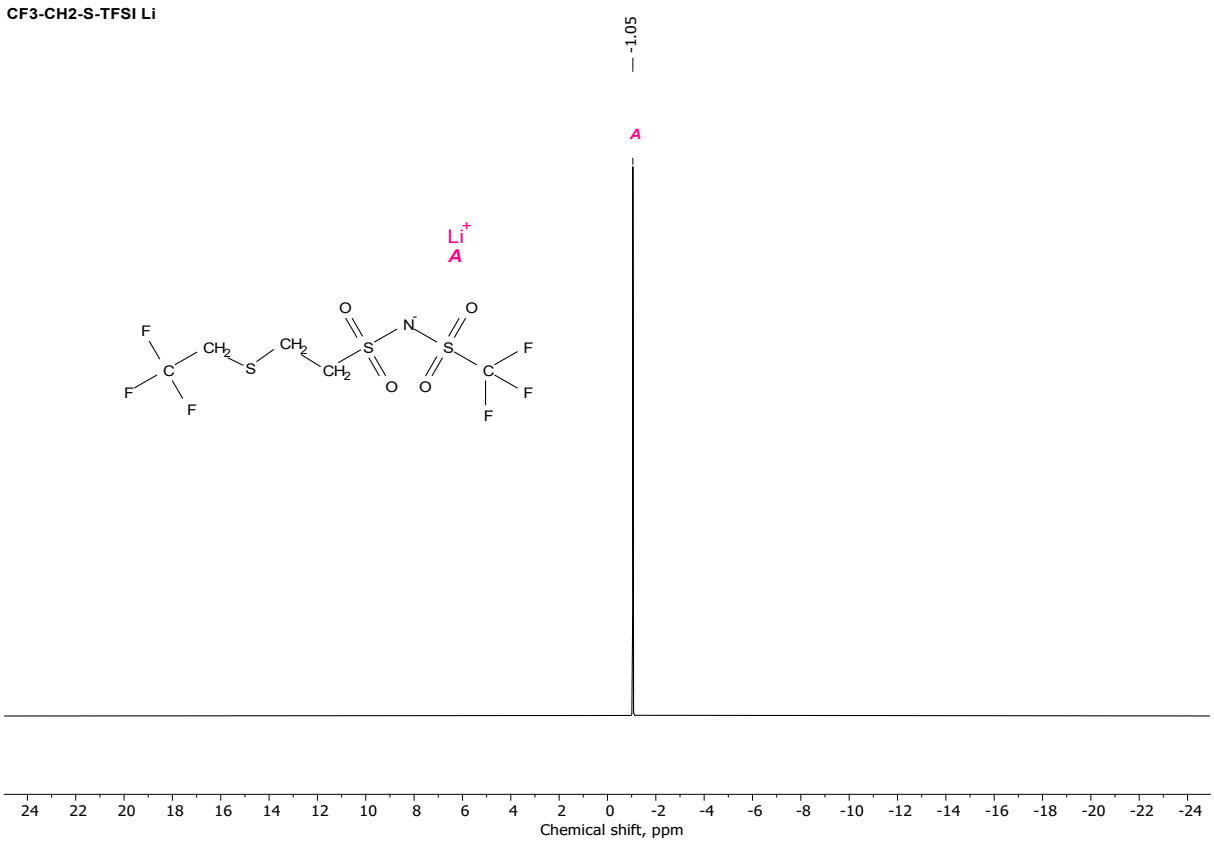

Figure S5. ^{7}Li NMR spectrum of **Li TFT-TFSI** (DMSO-d_6, 25.0 °C).

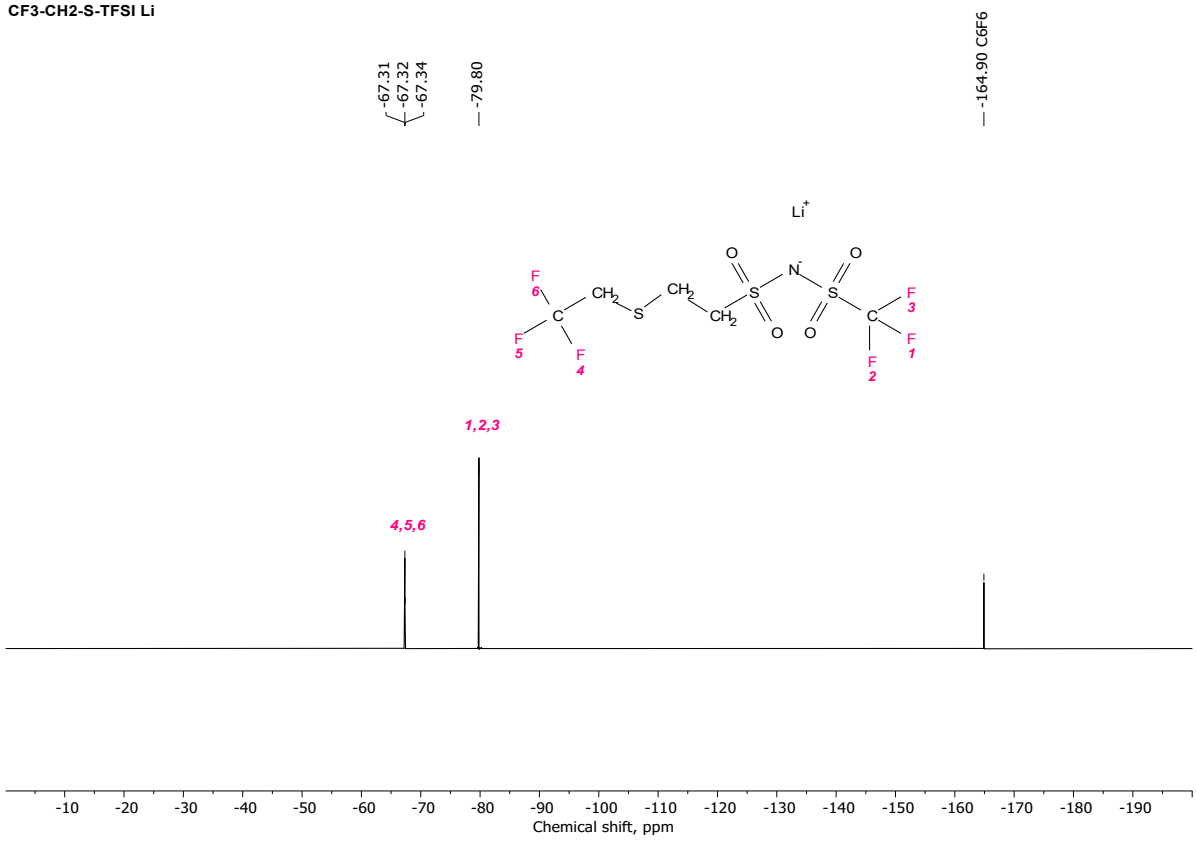

Figure S6. ^{19}F NMR spectrum of **Li TFT-TFSI** (DMSO-d_6, 25.0 °C).

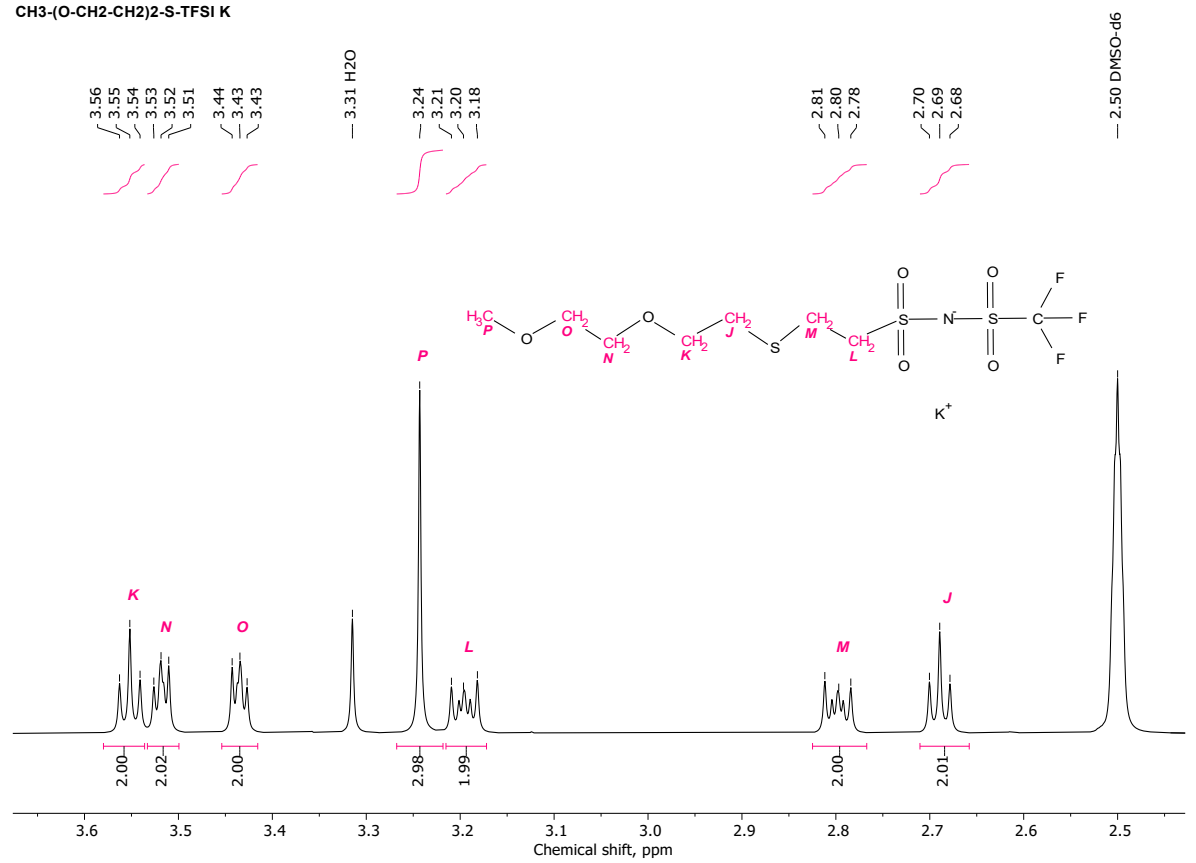

Figure S7. ^{1}H NMR spectrum of **CH_3-(O-CH_2-CH_2)$_2$-S-TFSI K** (DMSO-d_6, 25.0 °C).

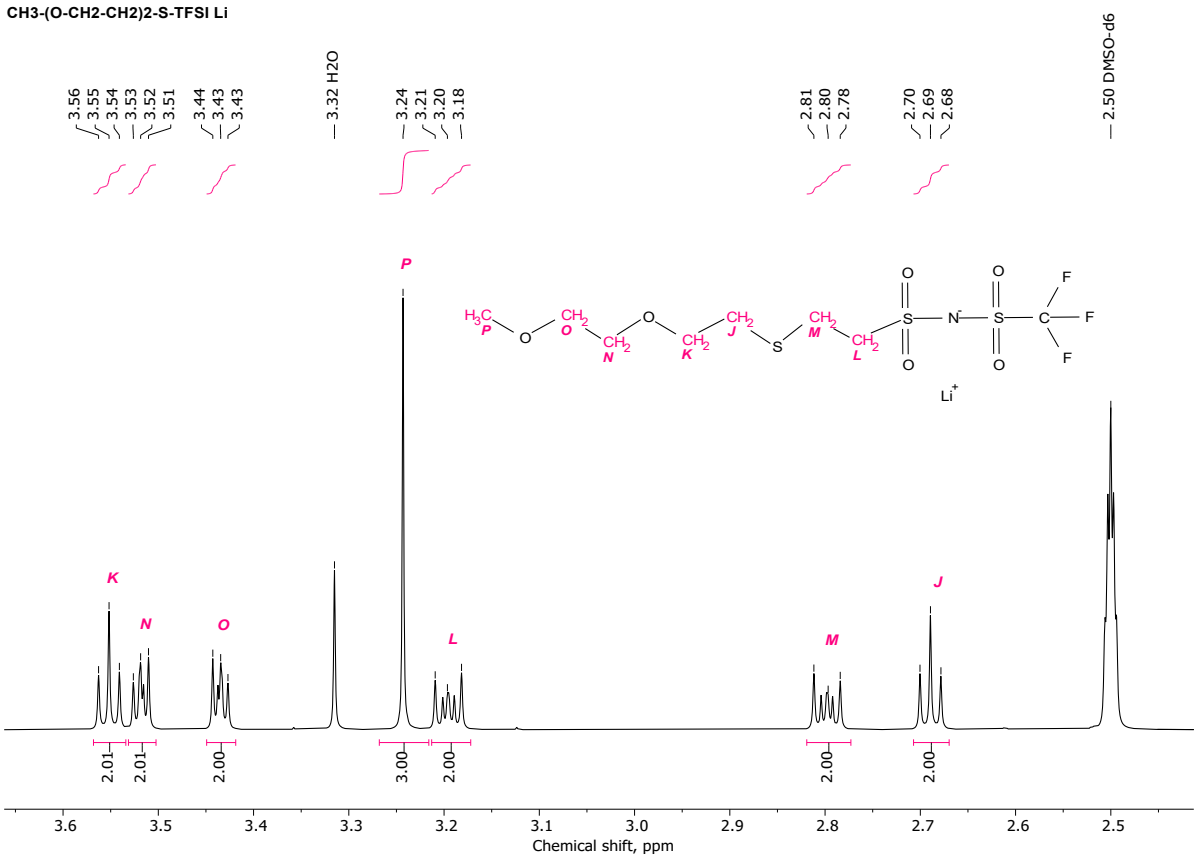

Figure S8. ^{1}H NMR spectrum of **Li MET-TFSI** (DMSO-d_6, 25.0 °C).

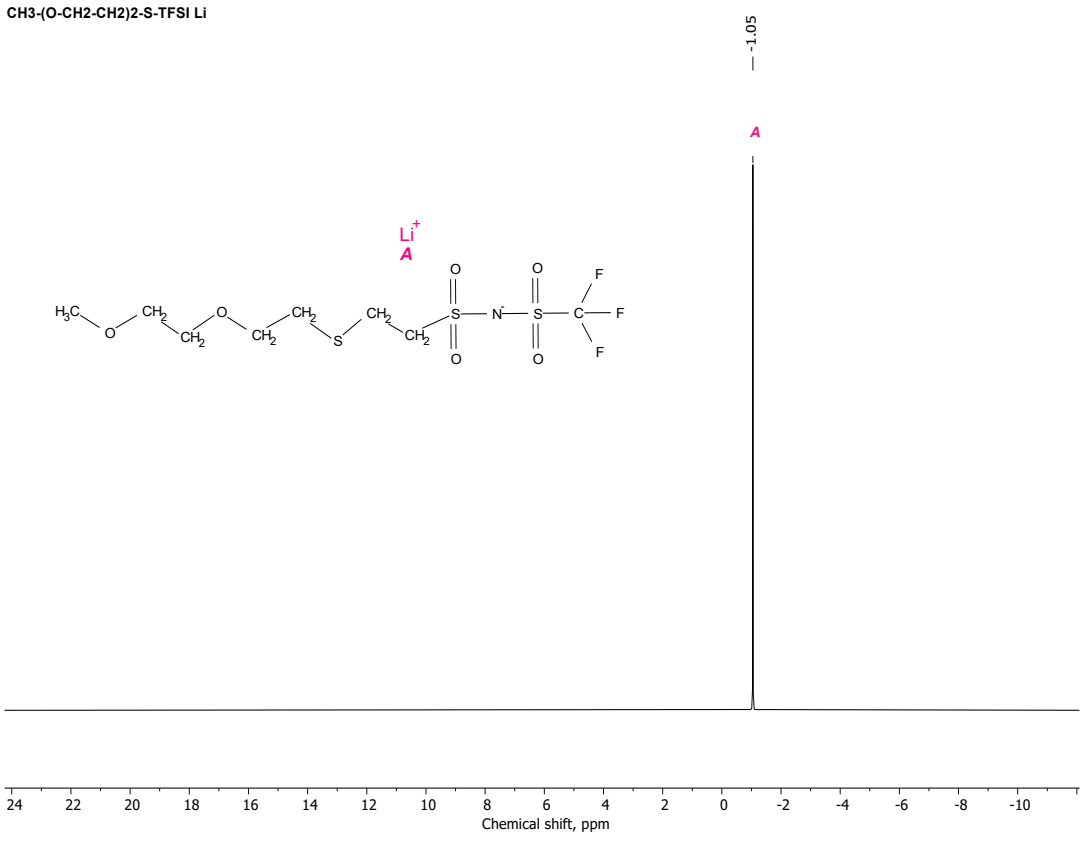

Figure S9. ^{7}Li NMR spectrum of **Li MET-TFSI** (DMSO-d_6, 25.0 °C).

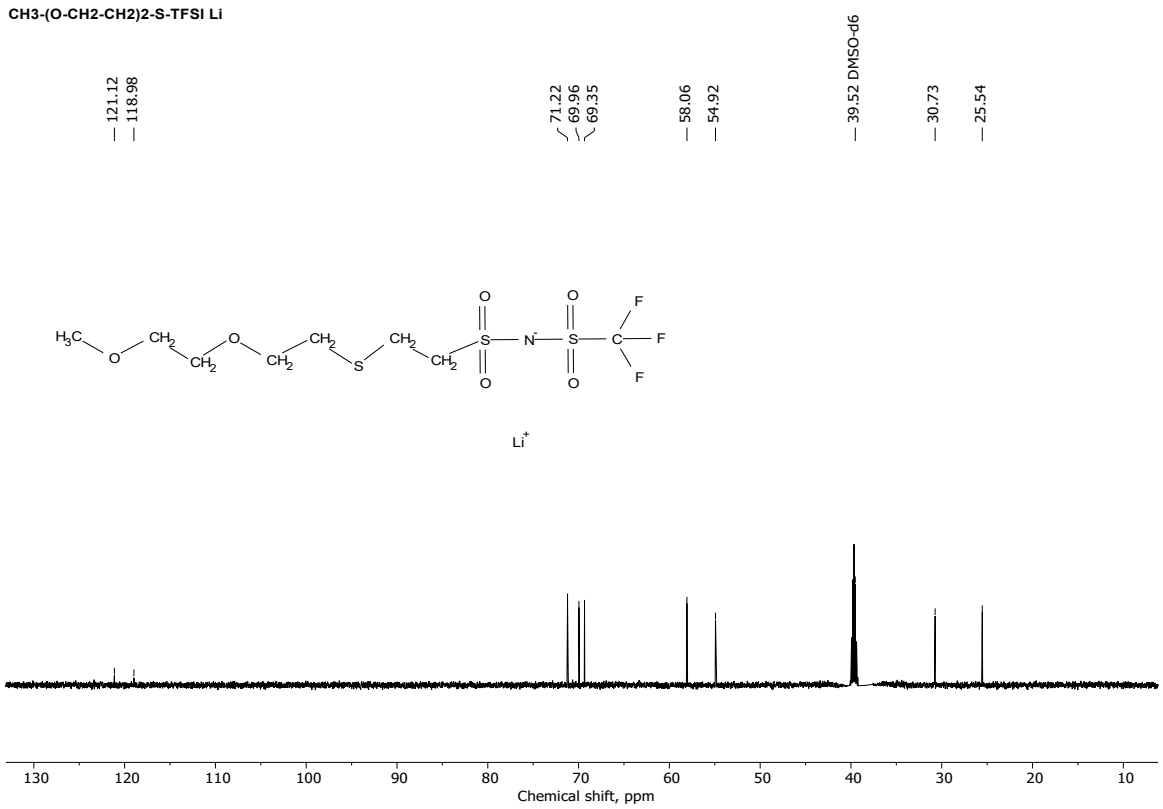

Figure S10. ^{13}C NMR spectrum of **Li MET-TFSI** (DMSO-d_6, 25.0 °C).

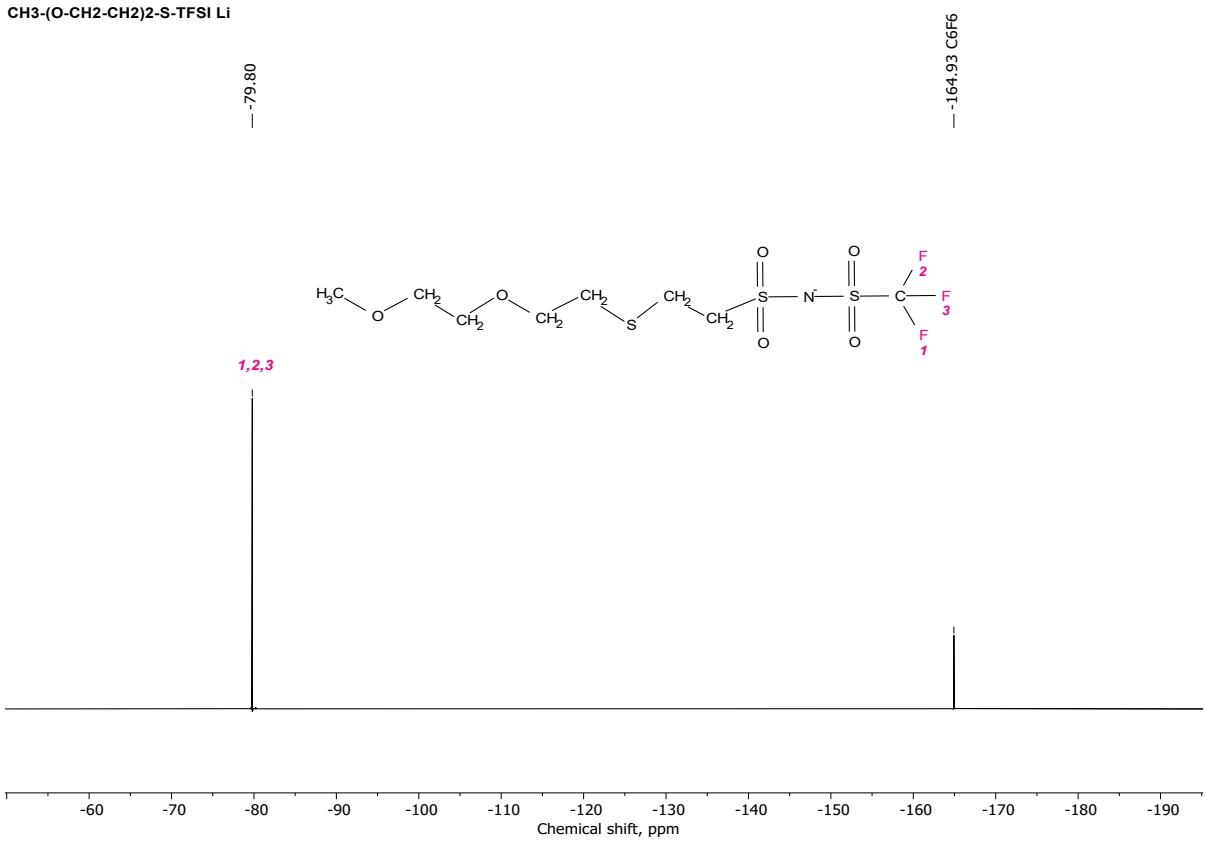

Figure S11. ^{19}F NMR spectrum of **Li MET-TFSI** (DMSO-d_6, 25.0 °C).

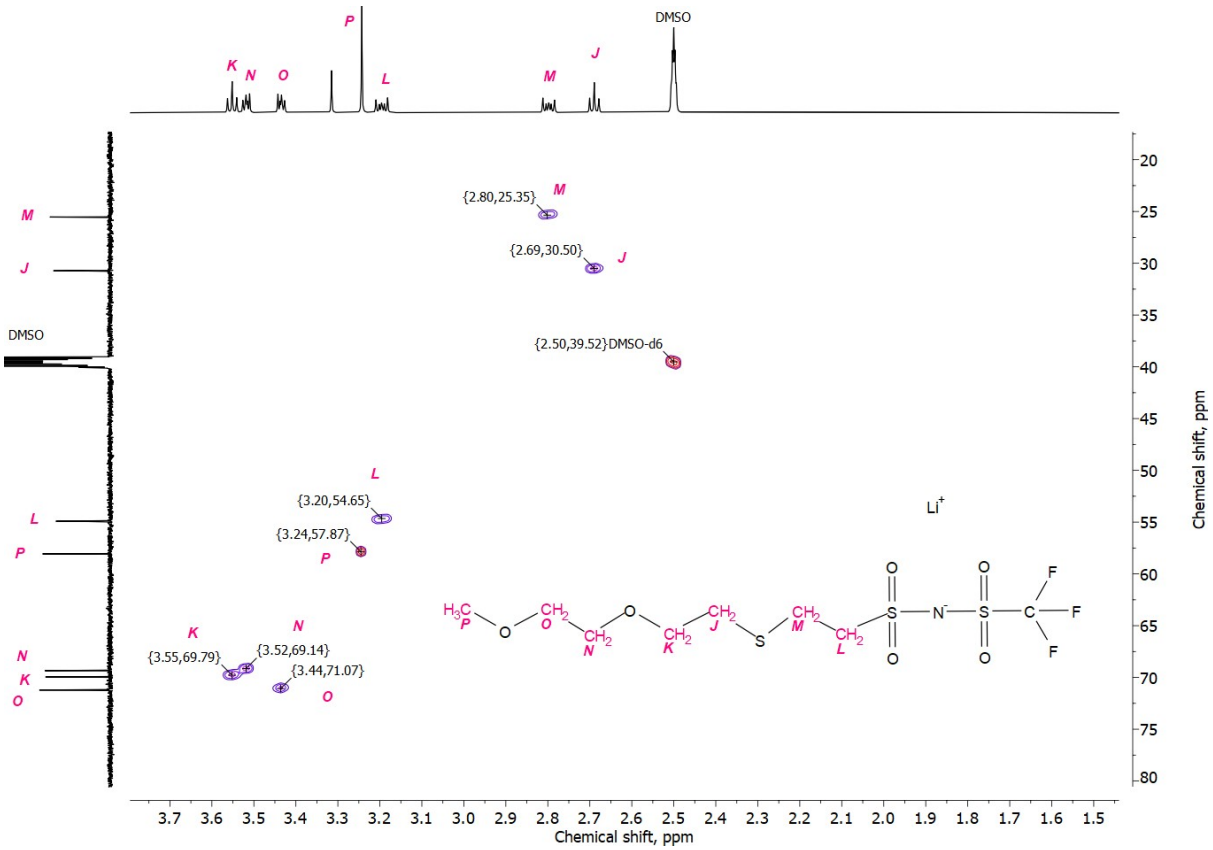

Figure S12. 2D HSQC spectrum of **Li MET-TFSI** (DMSO-d_6, 25.0 °C).

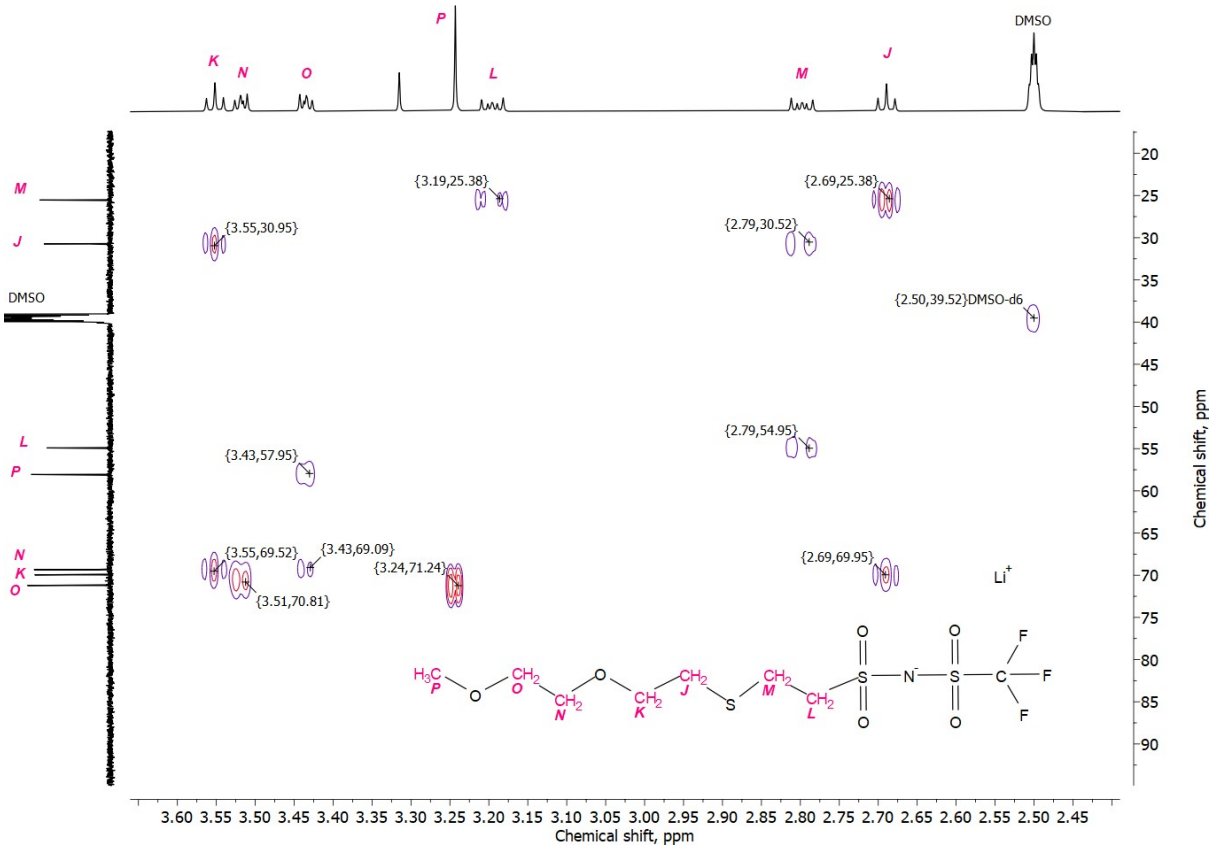

Figure S13. 2D HMBC Spectrum of **Li MET-TFSI** (DMSO-d_6, 25.0 °C).

Thermal Analysis

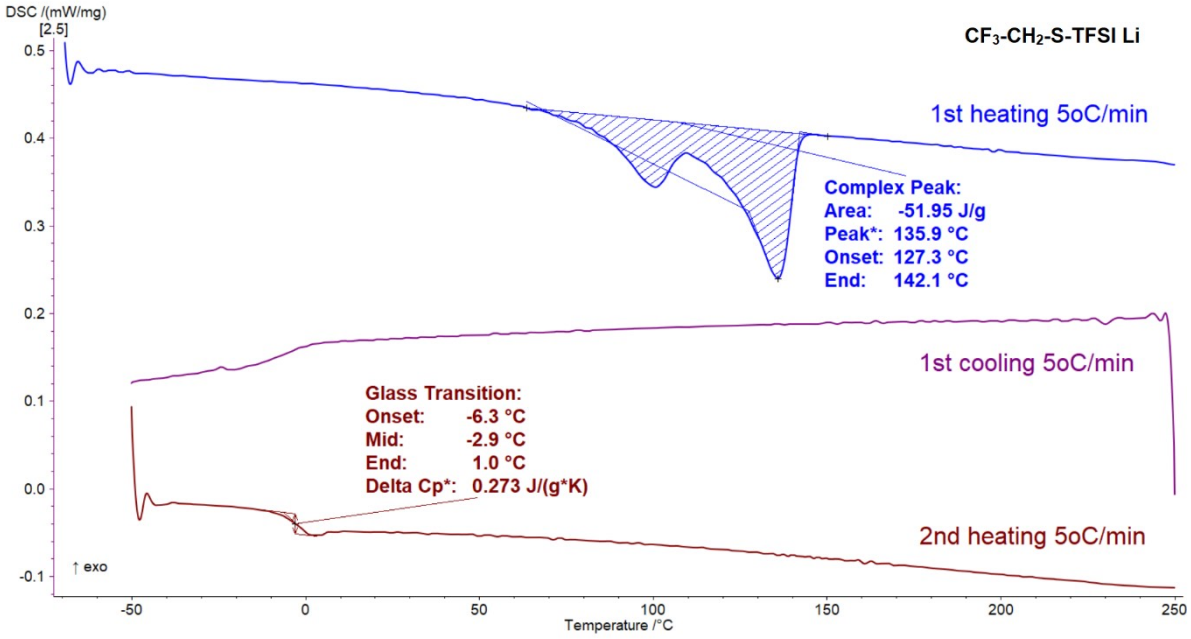

Figure S14. DSC curves of **Li TFT-TFSI.**

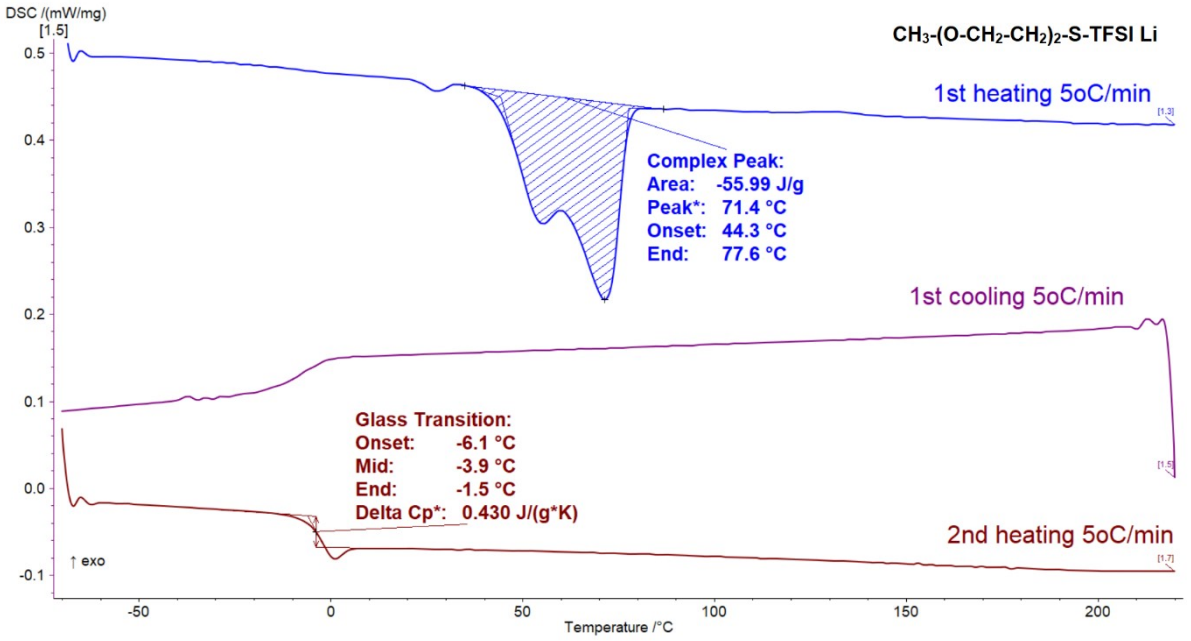

Figure S15. DSC curves of **Li MET-TFSI.**

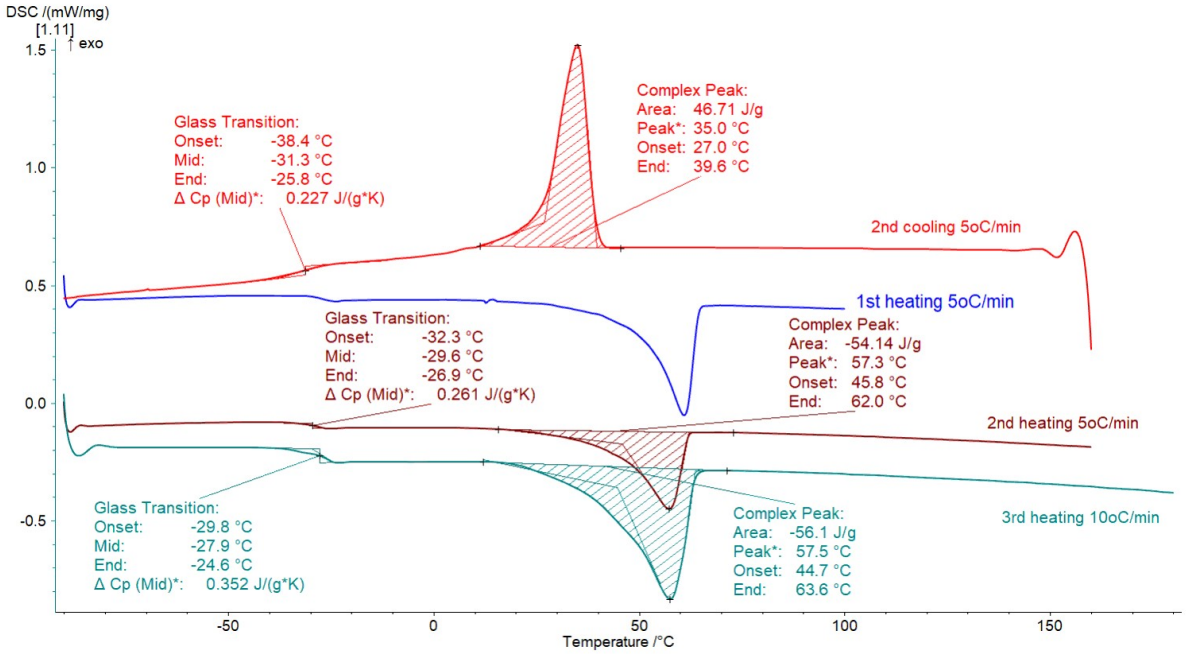

Figure S16. DSC curves of **Li TFT-TFSI/PEO.**

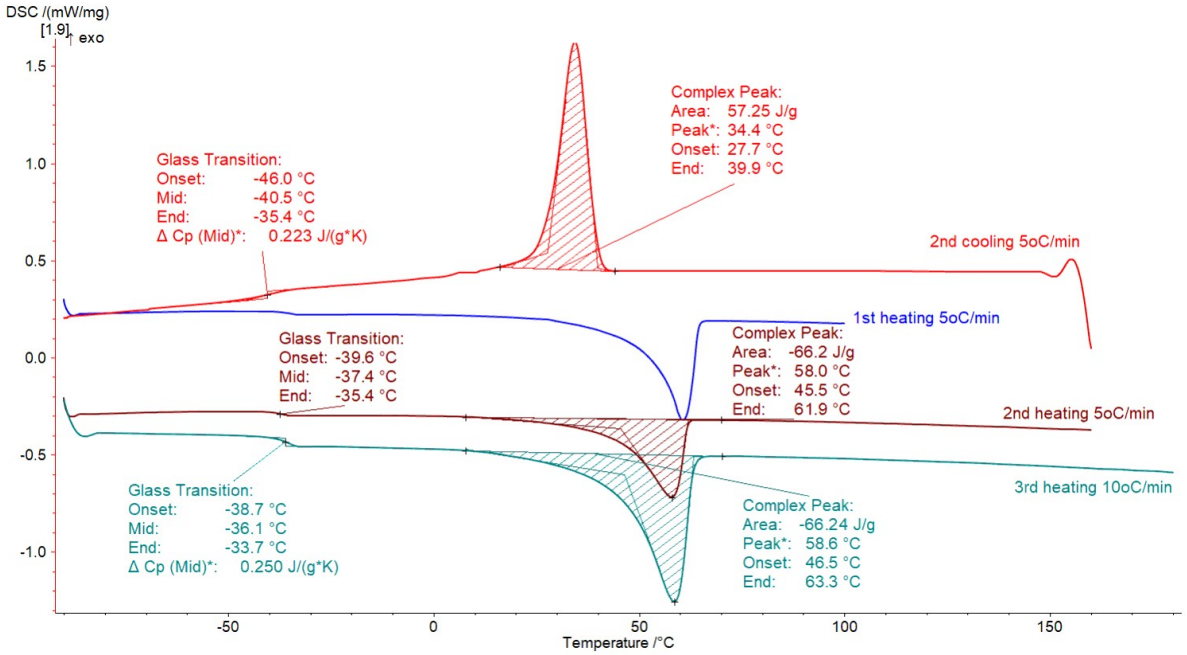

Figure S17. DSC curves of **Li MET-TFSI/PEO.**

Electrochemical analysis

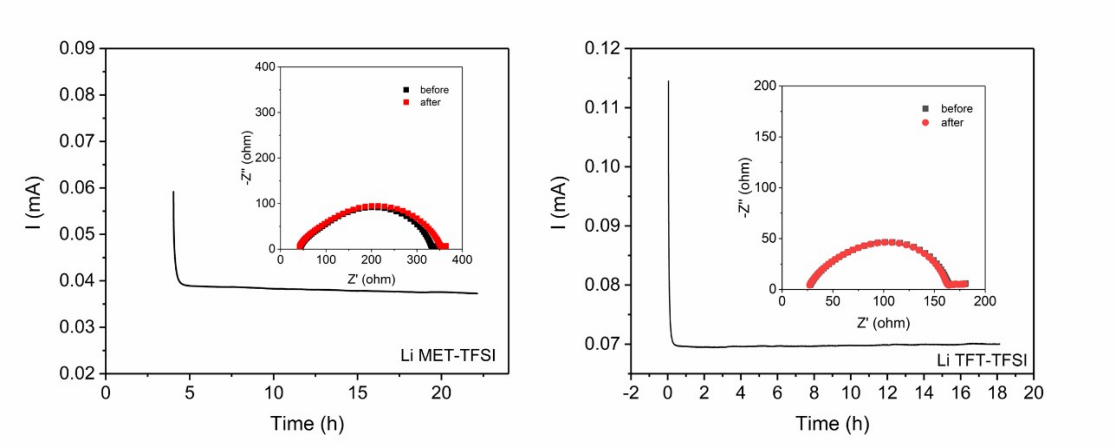

Figure S18. Lithium transference number measurements of **Li MET-TFSI/PEO** (left) and **Li TFT-TFSI/PEO** (right) at 70°C (EO/Li = 20), including chronoamperometry and EIS before and after polarization.

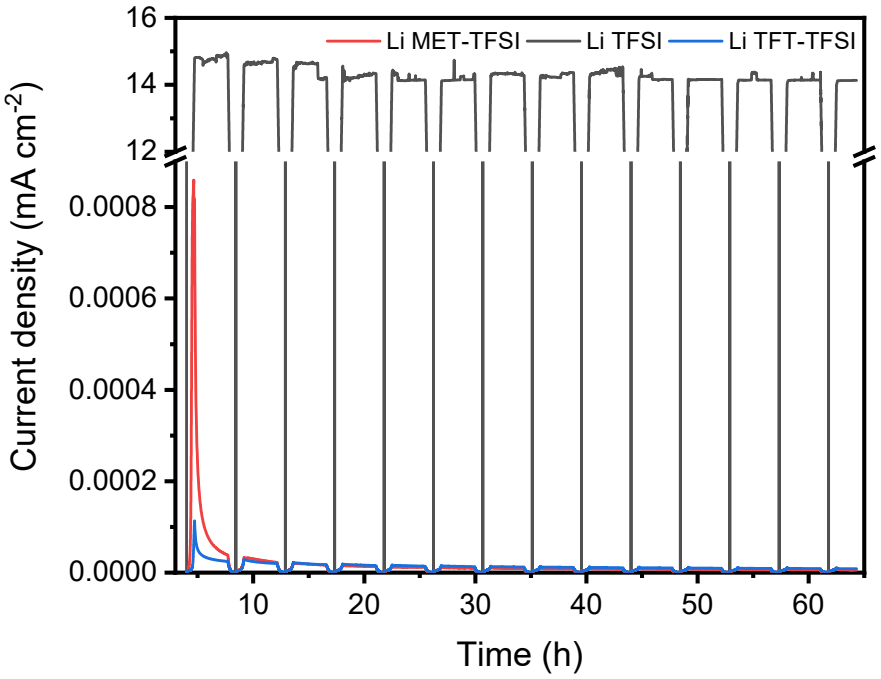

Figure S19. Anodic dissolution behavior of aluminum in 1 M **Li salt** in EC-DMC (1:1 v/v) liquid electrolytes measured in a two-electrode configuration (Al working electrode, activated carbon counter electrode) using a Whatman GF/A glass fiber separator.

XPS analysis

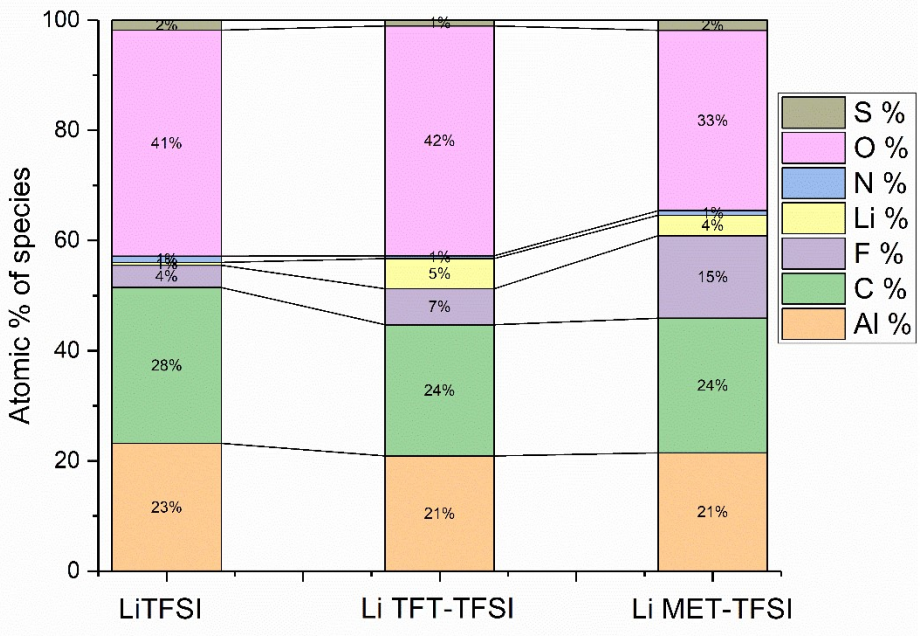

Figure S20. XPS surface elemental composition analysis of Al disks after anodic dissolution tests using LiTFSI (reference), **Li TFT-TFSI**, and **Li MET-TFSI** salts.

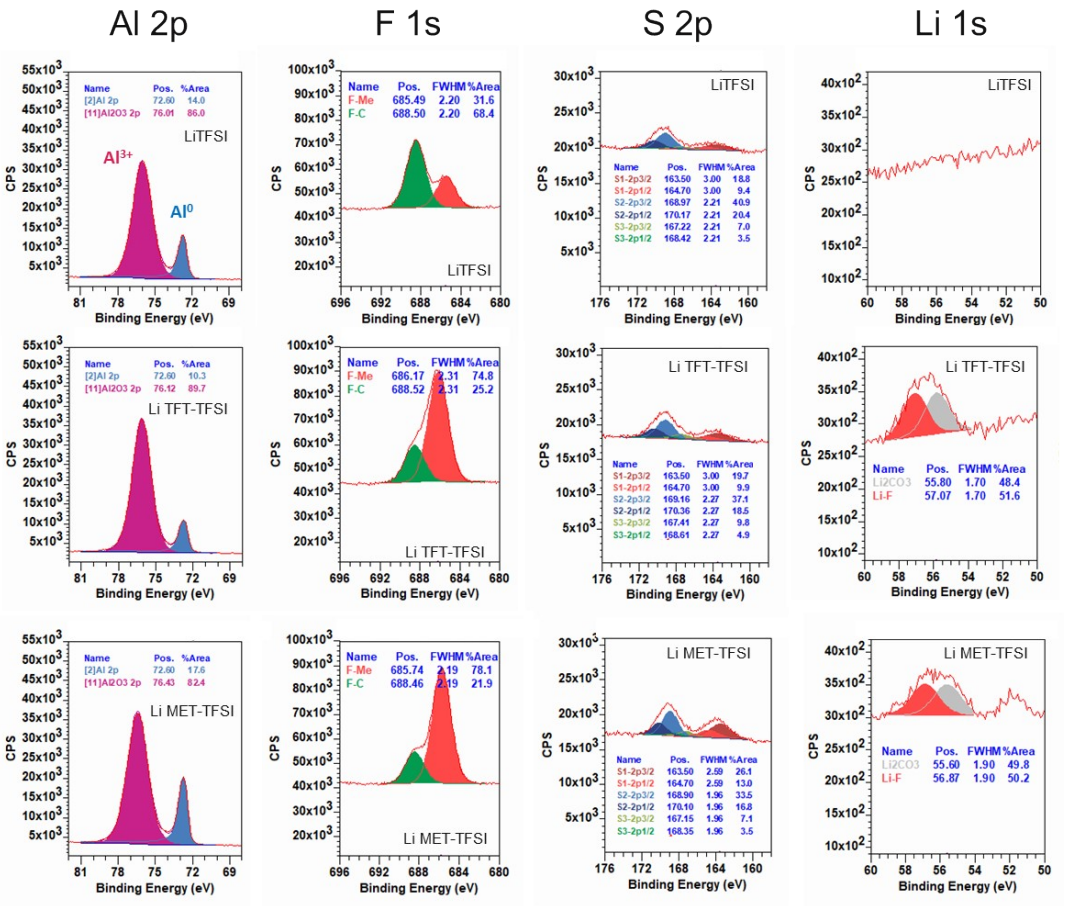

Figure S21. XPS core levels (Al 2p, F 1s, S 2p, and Li 1s) of Al disks after anodic dissolution tests using LiTFSI (up), **Li TFT-TFSI** (middle) and **Li MET-TFSI** (bottom) salts.

The surface elemental composition and corresponding XPS peak fitting of the Al 2p, F 1s, and S 2p regions (Figures S20–S21) consistently demonstrate that the nature of the interphase strongly depends on the Li salt employed in the electrolyte. In all cases, the detection of C, O, F, N, S, Li, and Al confirms the formation of a mixed organic/inorganic passivation layer arising from both solvent and salt decomposition.

For LiTFSI, the relatively high C and O contents, together with F 1s and S 2p signals dominated by components assigned to intact TFSI species, indicate that the surface layer is largely solvent-derived, with only a less contribution from salt decomposition. In contrast, electrolytes based on **Li TFT-TFSI** and, more prominently, **Li MET-TFSI** exhibit a marked increase in fluorine-containing species, consistent with a substantial contribution from salt decomposition. This trend is supported by the F 1s spectra, which show an increasing fraction of lower binding energy components attributed to metal fluorides (LiF and AlF_3), whereas the higher CF_x contribution observed for LiTFSI suggests partial preservation of the salt structure. In the S 2p region, a slight increase in lower binding energy components, likely associated with sulfite and SO_x species, is observed for **Li TFT-TFSI** and **Li MET-TFSI**. Among the three systems, **Li MET-TFSI** leads to the highest fluorine content and the most pronounced metal fluoride contribution in the passivation layer.

Overall, these results indicate that both **Li MET-TFSI-** and **Li TFT-TFSI-**based electrolytes promote the formation of a more fluoride-rich layer, with increased LiF and AlF_3 content, which is expected to provide enhanced protection of the aluminum surface against corrosion.

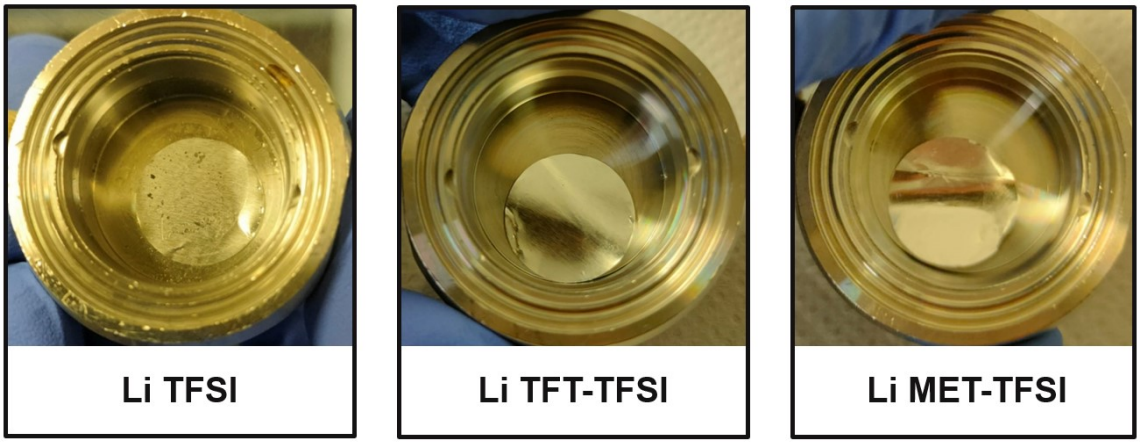

Figure S22. Digital photographs of aluminum disks after anodic dissolution tests in 1 M **Li salt**/EC–DMC (1:1 v/v) liquid electrolytes, showing visible corrosion pits on the Al surface in the presence of **LiTFSI**.

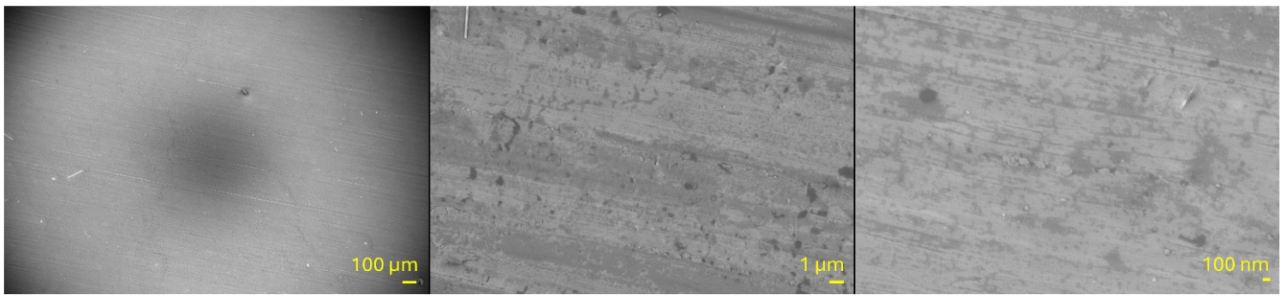

Figure S23. FESEM images of the Al disk surface after anodic dissolution test in 1 M **Li TFT-TFSI**/EC–DMC (1:1 v/v) liquid electrolyte.

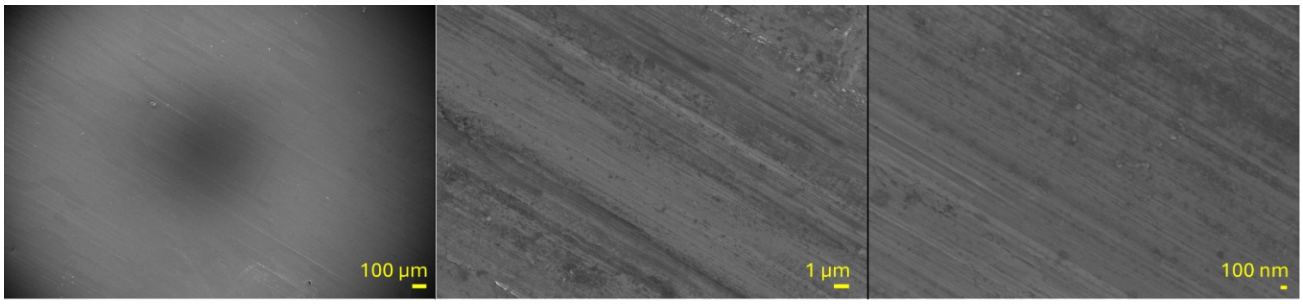

Figure S24. FESEM images of the Al disk surface after anodic dissolution test in 1 M **Li MET-TFSI**/EC–DMC (1:1 v/v) liquid electrolyte.

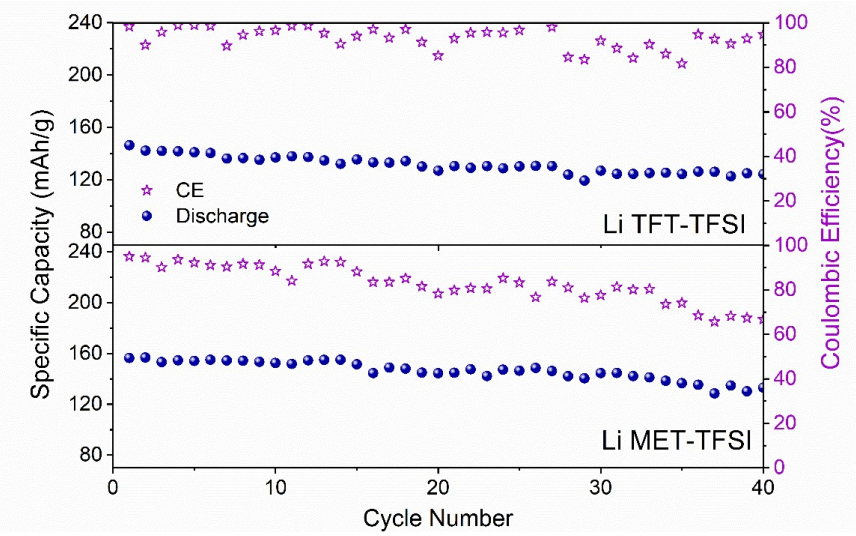

Figure S25. Specific capacity and coulombic efficiency as a function of cycle number for Li°‖**Li TFT-TFSI/PEO**‖$LiFePO_4$ (top) and Li°‖**Li MET-TFSI/PEO**‖$LiFePO_4$ (bottom) cells during galvanostatic cycling at C/15 and 70 °C.

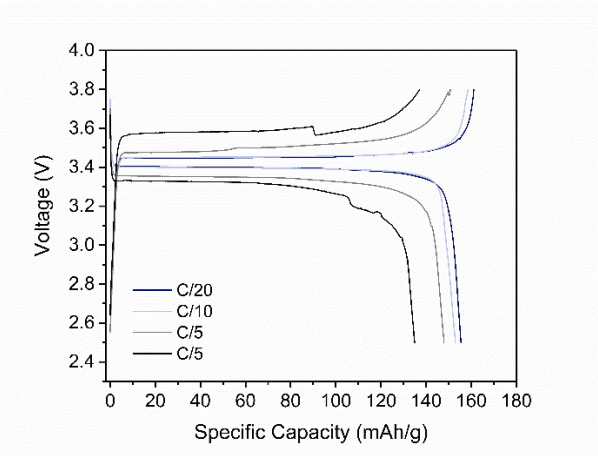

Figure S26. Potential vs. specific capacity profiles of Li°‖**Li TFT-TFSI/PEO**‖$LiFePO_4$ at 70 °C and variable C-rates.

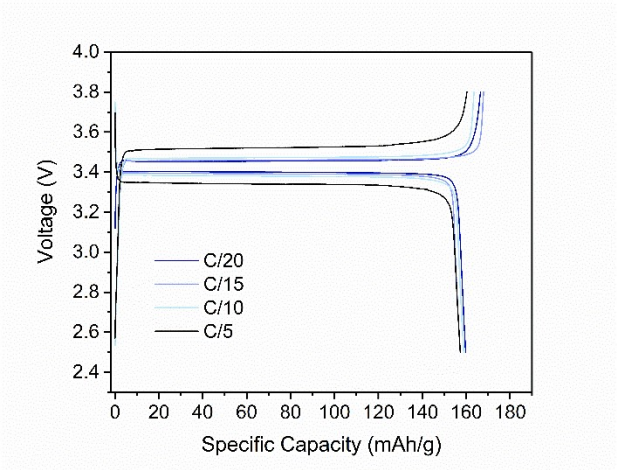

Figure S27. Potential vs. specific capacity profiles of Li°‖**Li MET-TFSI/PEO**‖$LiFePO_4$ at 70 °C and variable C-rates.

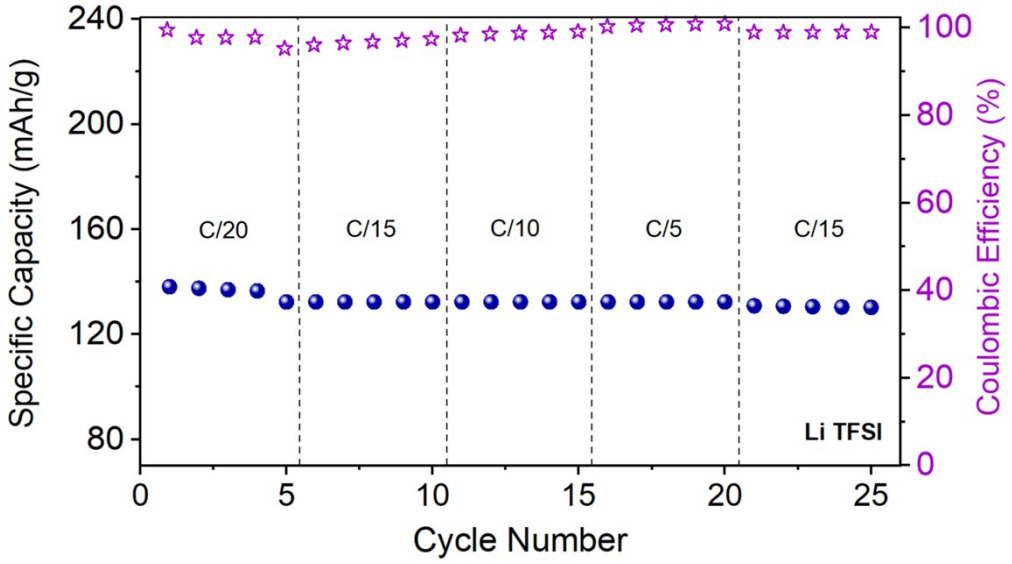

Figure S28. Specific capacity and coulombic efficiency as a function of cycle number for conventional Li°‖**Li TFSI/PEO**‖$LiFePO_4$ cell during galvanostatic cycling at 70 °C and variable C-rates.

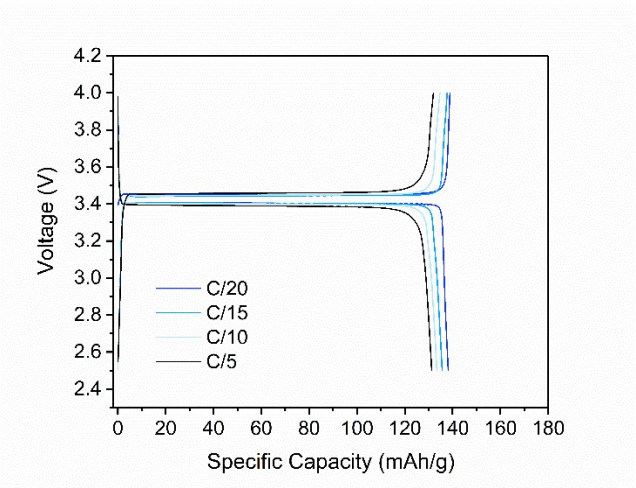

Figure S29. Potential vs. specific capacity profiles of Li°‖**Li TFSI/PEO**‖$LiFePO_4$ at 70 °C and variable C-rates.

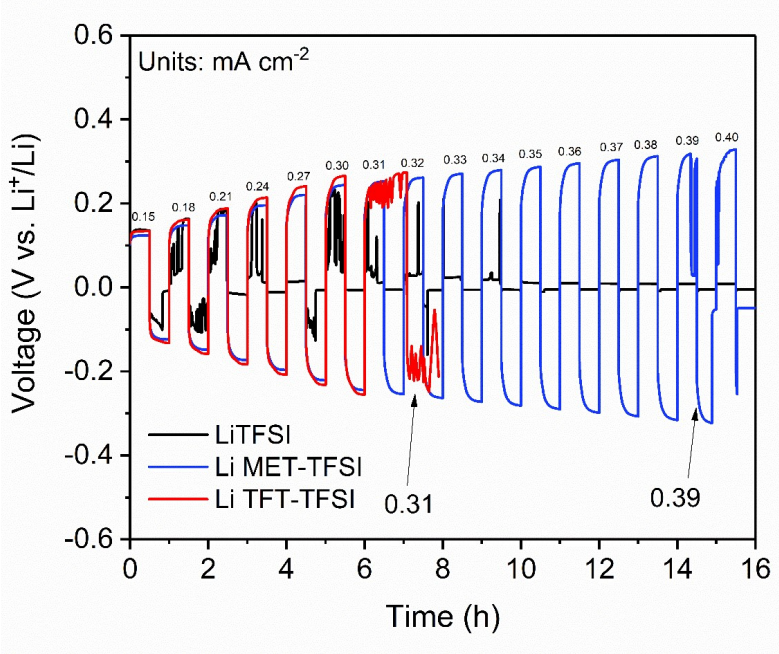

Figure S30. Critical current density (CCD) tests at 70 °C of symmetric Li°‖**Li salt/PEO**‖Li° cells. PEO/LiTFSI short-circuited after few cycles. **Li TFT-TFSI** and **Li MET-TFSI** SPEs sustained higher current densities and shorted at 0.31 mA cm^{-2} and 0.39 mA cm^{-2}, respectively.

REFERNCES

(1) Evans, J.; Vincent, C. A.; Bruce, P. G. Electrochemical Measurement of Transference Numbers in Polymer Electrolytes. *Polymer* **1987**, *28* (13), 2324–2328. https://doi.org/10.1016/0032-3861(87)90394-6.

(2) Bhowmick, S.; Ahmed, M.; Filippov, A.; Loaiza, L. C.; Shah, F. U.; Johansson, P. Ambient Temperature Liquid Salt Electrolytes. *Chem. Commun.* **2023**, *59* (18), 2620–2623. https://doi.org/10.1039/D3CC00318C.

(3) Żukowska, G. Z.; Piszcz, M.; Gańko, K.; Więckowski, M.; Królikowski, M.; Poterała, M.; Dranka, M. Basic Properties of Glyme-Based Electrolytes Doped with Lithium 2,4,5-Tricyanoimidazolide (LiTIM). *Mater. Chem. Phys.* **2024**, *315*, 128999. https://doi.org/10.1016/j.matchemphys.2024.128999.

(4) Fraile-Insagurbe, D.; Meabe, L.; Fortuin, B. A.; Segura-Laparra, I.; Sasieta-Barrutia, E.; Cid, R.; Carrasco, J.; Wieczorek, W.; Forsyth, M.; Armand, M.; Martínez-Ibañez, M. Toward Safer and Sustainable Lithium Metal Batteries: Fluorine-Free Solid Polymer Electrolytes. *Energy Environ. Mater.* **2026**, e70271. https://doi.org/10.1002/eem2.70271.

(5) Xu, W.; Angell, C. A. Weakly Coordinating Anions, and the Exceptional Conductivity of Their Nonaqueous Solutions. *Electrochem. Solid-State Lett.* **2001**, *4* (1), E1. https://doi.org/10.1149/1.1344281.

(6) Xu, R.; Xiao, B.; Xuan, C.; Gao, S.; Chai, J.; Liu, S.; Chen, Y.; Zheng, Y.; Cheng, X.; Guo, Q.; Liu, Z. Facile and Powerful In Situ Polymerization Strategy for Sulfur-Based All-Solid Polymer Electrolytes in Lithium Batteries. *ACS Appl. Mater. Interfaces* **2021**, *13* (29), 34274–34281. https://doi.org/10.1021/acsami.1c07805.

(7) Xuan, C.; Gao, S.; Wang, Y.; You, Q.; Liu, X.; Liu, J.; Xu, R.; Yang, K.; Cheng, S.; Liu, Z.; Guo, Q. In-Situ Generation of High Performance Thiol-Conjugated Solid Polymer Electrolytes via Reliable Thiol-Acrylate Click Chemistry. *J. Power Sources* **2020**, *456*, 228024. https://doi.org/10.1016/j.jpowsour.2020.228024.

(8) Sarapas, J. M.; Tew, G. N. Poly(Ether–Thioethers) by Thiol–Ene Click and Their Oxidized Analogues as Lithium Polymer Electrolytes. *Macromolecules* **2016**, *49* (4), 1154–1162. https://doi.org/10.1021/acs.macromol.5b02513.